2019-01-01

Investigating Using Titanium Zirconium Molybdenum for Additively Manufacturing Aerospace Components

Justin Hunter Vanhoose
University of Texas at El Paso

INVESTIGATING USING TITANIUM ZIRCONIUM MOLYBDENUM FOR ADDITIVELY MANUFACTURING AEROSPACE COMPONENTS

JUSTIN H. VANHOOSE

Master's Program in Mechanical Engineering

APPROVED:

Ahsan R. Choudhuri, Ph.D., Chair

Ryan Wicker, Ph.D., Co-Chair

Jack F. Chessa, Ph.D.

Tzu-Liang (Bill) Tseng, Ph.D., CMfgE

Stephen Crites, Ph.D.
Dean of the Graduate School

Dedication

I dedicate this thesis to all of my family, friends, professors, and colleagues that I have had the pleasure and privilege to get to know along the way.

INVESTIGATING USING TITANIUM ZIRCONIUM MOLYBDENUM FOR ADDITIVELY MANUFACTURING AEROSPACE COMPONENTS

by

Justin H. Vanhoose, B.S. Engineering/Physics

THESIS

Presented to the Faculty of the Graduate School of

The University of Texas at El Paso

in Partial Fulfillment

of the Requirements

for the Degree of

MASTER OF SCIENCE

Department of Mechanical Engineering

THE UNIVERSITY OF TEXAS AT EL PASO

August 2019

Acknowledgements

I would like to thank Valley Tech Systems for funding this effort. The material covered in this thesis is on work supported by VTS-Refractory Additive Manufacturing Program Code: 21809, SOW No.: 21809-00020-01. Any findings, conclusions, opinions or recommendations presented in this thesis do not directly reflect the views of Valley Tech Systems. I would like to thank Charles Scott Hill. Mr. Hill taught me how to have passion for the aerospace industry and engineering. I would like to thank my advisor, Dr. Ahsan Choudhuri for providing me the opportunity to work and flourish in his research center. I would like to thank Dr. Ryan Wicker for allowing me to conduct research in his center for this effort. I would like to thank all of my teammates, administration staff, and research engineers at the Center for Space Exploration and Technology Research. A special thank you goes to my family and friends whom have supported me throughout the tenure of my education. I would like to finally acknowledge Dr. Abdel Bachri from Southern Arkansas University. Without him taking an interest and pushing me through my undergraduate years, I would never have become an engineer and a steward of science.

Table of Contents

List of Figures

List of Tables

Chapter 1: Introduction

Mankind throughout history has possessed an innate characteristic to explore, migrating to new frontiers. The requirement for this travel is most broadly associated with the need to pursue more resources. One of the earliest recorded examples of this occurred over 40,000 years ago when hunters crossed from Asia to America on a land bridge, following animal trails [1].

"I look toward the fields at the east," Robert Goddard has been quoted, "imagining how wonderful it would be to make some device which had even the possibility of ascending to Mars." [2] Goddard is not the only person to have thoughts of exploring. History has been rich of discovering lands, faring seas, conquering harsh environments, and has now moved on to space travel. Rockets have been used as a means of weapons since the Sung Dynasty in the 13th empire and have now been integrated for travel/transport [3]. The sophistication of rocketry and propulsion has reached a level to where it is plausible that mankind will be a multiplanetary species.

The space industry has grown significantly with the advancement of the sophistication of these rocket technologies. SmarTech Publishing expects the industry to grow to a staggering worth of 330 billion dollars within the next decade [4]. This growth can be credited to commercialization of the space industry as independent companies compete with one another to drive down costs and develop new materials and technologies.

The specific challenge to overcome in space travel is how high the cost is per kilogram to escape the Earth's atmosphere. Currently, to achieve Low Earth Orbit, it costs roughly $2,500/kg on the SpaceX Falcon 9 [5]. Keep in mind that this is the gross cost per kilogram of payload for the vehicle. SpaceX as a company would charge their customers significantly more.

SmarTech Publishing stated in an economic evaluation of the space industry that additive manufacturing, (AM) will play a key role in the up and coming space market. AM has a proven history of lowering cost of manufacturing as well as driving efforts for advancements in new materials [6]. Because of this, AM could potentially be the most effective tool at addressing the high cost per kilogram issue.

Combined with the growth of the space industry in parallel to AM being able to help with the high costs of space travel, it can be speculated that there is a need for AM in aerospace. The focus of this thesis is on developing methods of AM of aerospace components with refractory metals, specifically Titanium Zirconium Molybdenum, (TZM). This thesis covers the initial stages of this effort as it is being conducted at the University of Texas at El Paso.

1.1 Relevance of the Project in the Space Industry

One of the most important events throughout history was the Apollo Moon landing. In 1969, the world would change as the Lunar Lander descended upon the surface of the Moon, followed by Neil Armstrong's iconic line, "That's one small step for [a] man, one giant leap for mankind."

Since the launch of Sputnik in October of 1957, there have been more than 6,000 satellites that have departed from Earth [7]. The humble beginning of space travel has gone from a few missions to an ever growing need to occupy Low Earth Orbit (LEO) and beyond.

One of the glaring questions the space industry is subjected to is necessity. People are generally skeptic in investing so much time and money to leave Earth. One simple but effective answer is resources. "The economic development hinges on an ability to utilize what we term space resources," stated in a publication titled "*New Policies Needed to Advance Space Mining*" [8]. Within the reaches of the inner solar system lies a vast array of resources that far outnumber those available on Earth. For example, an asteroid named "16 Psyche" (discovered by Annibale de Gasparis in 1852) has an estimated radius of 112.5 km, and is expected to be composed of ninety percent Iron [9].

Developing technologies, communications, and national security are other reasons why space travel has become essential. Italian Physicist Giovanni Bignami once wrote, "Without astronauts and their cheering crowds to rally us along, space applications and space science will quickly wither into oblivion. Forty years from now there will be no space activities at all if we do not send people beyond Earth's orbit, where no one has been since 1972" [10].

Private space venturing companies such as the United Launch Alliance (ULA) are restructuring themselves to address the needs and importance of the space market. The ULA has an on-going effort to reduce costs associated with launching vehicles by implementing AM. The ULA also

desires to broaden the capabilities of these vehicles while developing their next generation "*Vulcan Centaur*" from more than 120 years of launch experience [11]. "If you can design it, we can produce it," stated ULA engineer G.J. Schiller in an IEEE Aerospace Conference Paper. Referring to AM for ULA's futuristic technologies, Schiller also stated, "No longer is the aerospace engineer constrained by the ability to manufacture a component" [11].

Taking in all accounts of necessity, growth of the market, and sustaining continual developments in space travel, it is easy to see the importance of AM. The University of Texas at El Paso is interested in contributing to these exploits by developing printing processes of TZM and other refractory metals. With these developments, it is believed that UTEP can have a claim in the growing space industry.

1.2 Brief Introduction of Additive Manufacturing

AM is a process in which layers of material are selectively positioned and laminated together to form three-dimensional objects. This technology is beneficial because it allows for components to be fabricated that would not normally be possible by conventional manufacturing. According to NASA's presentation, "*Additive Manufacturing of Aerospace Propulsion Components*," their rocket propulsion systems utilizing AM had greater cycle time, more feasibility of implementing complex designs, and a significant reduction in fabrication time [12]. Systems designed for the NASA-Air Force-Aerojet Collaborative Effort initially had lead times estimated to up to one year for their components. However, by implementing an AM process, the effort was able to decrease lead times to only four months. Greater design complexities and reduced fabrication time and waste are made possible from shape-optimization softwares incorporated by most AM processes [12].

This effort will be using an AM process called Powder Bed Fusion (PBF). PBF takes particles of metal, roughly 10-50 microns in diameter, and selectively sinters or melts them together, via a plasma laser or electron beam [13]. This allows for designs to be fabricated without a large sum of steps for post-processing. The following figure depicts the PBF process [8].

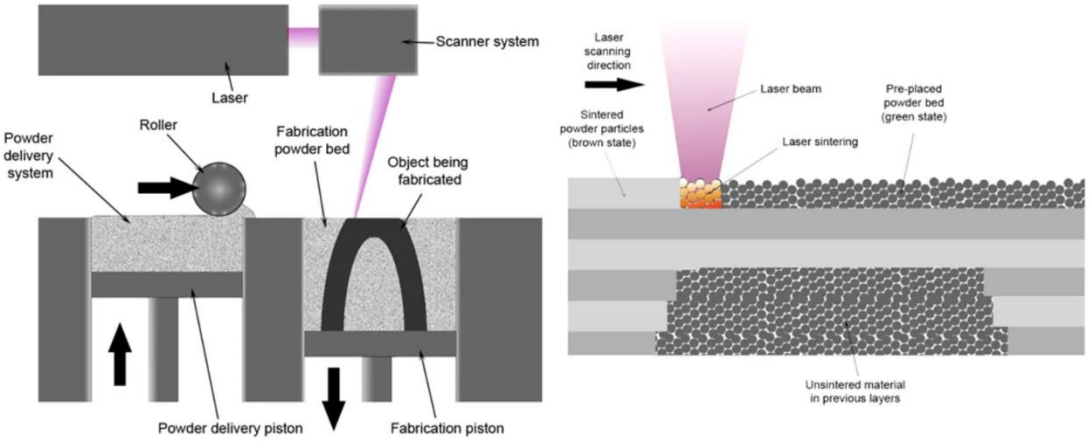

Figure 1: General Process of AM (PBF)

There are two main categories of PBF, Selective Laser Melting (SLM) and Electron Beam Melting (EBM) [13]. EBM fuses together metal particles or wire with an electron beam in vacuum. Typically, EBM is a faster process than SLM, however the tradeoff is an increase in surface roughness in the printed parts.

SLM uses a high-density laser to fuse/melt particles in the print bed together. This application is better suited for more complex geometries having thinner walls/channels. Although SLM has a slower build rate then EBM, due to the flexibility with geometry complexity and finer surface finishes of printed components, it is the method of choice in this research [13]. It is the goal of the research team at UTEP to use SLM to investigate AM aerospace components out of TZM.

1.3 Titanium Zirconium Molybdenum

Titanium Zirconium Molybdenum (TZM) was developed by Climax Molybdenum Co. in 1954. It is the most widely used alloy of Molybdenum and is typically implemented in environments that have high temperature loadings such as furnace components, die inserts for casting, hot stamping tooling, rocket nozzles, and electrodes [14]. Molybdenum is a natural resource in the United States and is cheaper than most refractory metal [15]. TZM is composed of amounts of the following elements [19].

Table 1: Chemical Composition of TZM

TZM Chemical Composition:

Element	Content (%)
Molybdenum, Mo	99.40
Titanium, Ti	0.5
Zirconium, Zr	0.08
Carbon, C	0.02

It is important to note that TZM is slightly over ninety percent Molybdenum. Molybdenum has a high melting point, 2,600 degrees Celsius. For reference, the melting point of most Inconel alloys is around 1,300 degrees Celsius. Molybdenum has the desirable characteristic to be able to withstand high temperatures without expanding or softening significantly [16]. Molybdenum in its pure form has one of the lowest thermal expansion coefficients of all metals used in commercial environments. In many alloys of steel, Molybdenum is credited for increasing hardenability, strength, toughness, and resistance to wear/corrosion [16].

TZM has all of the positive properties that are desirable in Molybdenum, while also having nearly twice the strength and a much higher recrystallizing temperature (1,025 degrees Celsius) [17]. This is attributed to the Titanium and Zirconium carbide bonds in TZM. These carbide bonds allow for TZM to have a finer grain structure when compared to pure Molybdenum, that inhibit grain growth during thermal or physical loadings [17]. These same carbides that help with the strength of the

material precipitate during the manufacturing process of TZM, that ultimately inhibit recrystallization. Following are tables displaying the physical properties of TZM [19].

Table 2: Physical Properties of TZM

TZM Physical Properties:

Density	Lb/in^3	0.37
	Gm/cm^3	10.22
Melting Point	°F	4753
	°C	2623
Thermal Conductivity	$Cal/cm^2/cm°C/sec$	0.48
Specific Heat	Cal/gm/°C	0.073
Coefficient of Linear Thermal Expansion	Micro-in/°F x 10^{-6}	2.50
	Micro-in/°C x 10^{-6}	5.20
Electrical Resistivity	Micro-ohm-cm	6.85

Table 3: Mechanical Properties of TZM

TZM Mechanical Properties:

Yield Strength	PSI	87,000
Ultimate Tensile	PSI	100,000
Hardness	DPH	220

As can be seen in the previous tables, TZM has relatively the same melting point, thermo-conductivity, density, and other thermal parameters as Molybdenum. Where the two differ drastically is in mechanical properties with TZM being much stronger. All of these properties considered is why TZM was picked as the material used for this effort.

1.4 Project Relevance

As discussed previously, there is a prominent growth in the space industry directly related to commercialization. With this growth comes a need to develop new technologies, materials, and methods that allow for industrial type companies to compete with one another. This competition is the driving force behind achieving new feats in the era of space travel.

This project is relevant to the space industry because it applies AM, a proven method to reduce cost, weight, waste, and lead times, with a material that has properties suitable for aerospace. Being able to create a process to AM aerospace components with TZM will be cutting edge and lead to further sources of funding, research, and partnerships at UTEP.

1.5 Project Objectives

The main objective of this project is to develop an AM process to make aerospace components out of refractory metals. Specifically, this thesis covers the beginning stages of researching the feasibility of using TZM.

The initial goal of this research was to validate the use of TZM in the harsh environments that are characteristic to aerospace. This was done by investigating if TZM had been used for aerospace components in the past. Next, the properties of TZM were evaluated and compared to other alloys that had been previously printed successfully in order to establish confidence that TZM could be used in AM.

After the initial investigations, the next goal was to develop a printing campaign that verified the printability of the material as well as produced components that could be subjected to post-printing analysis. The analysis allowed the team to hone in on ideal printing parameters of TZM. The details of the initial research, print methodologies, post print results and analysis, and over all findings are discussed further in depth in the proceeding sections.

Chapter 2: Background and Theory

The beginning work of this effort was to provide enough supporting evidence that TZM could not only be used in the harsh environment aerospace components are subjected to, but also if it is suitable for an AM process. This was done by conducting a thorough literature review of TZM and its history of uses. As discussed in the introduction, TZM is the most widely used alloy of Molybdenum. Like Molybdenum, TZM has several thermal and mechanical properties that are desired in the aerospace industry.

Initially the type of components that are to be manufactured in this effort are small thrusters (one-twenty newton range). Later on, research will be conducted in manufacturing larger scale components such as propellant tanks for CubeSats, smart propellant injectors, sealing surfaces, and other components. However, before any of these specimens can be printed, there is need for identifying ideal printing parameters for the alloy, as well as doing other analysis and testing to compare the features of printed TZM to solid TZM.

2.1 Investigations of TZM in Aerospace

Initial validations of selecting TZM were done by first seeing if the alloy had a history of previous use in aerospace. Gordon L. Cann filed a patent for a Spacecraft Optimized ARC Rocket that had capabilities of heating fluids to 1,000 degrees Celsius. This craft was specifically designed as a thruster for orbital positioning of satellites and space vehicles [20]. The thruster works by utilizing an enclosed arc to heat propellants, inhibiting an expansion that results in thrust. Cann incorporated Molybdenum and TZM for walls of the chamber, the nozzle inlet, and the expansion nozzle itself. This was done because of the mechanical and thermal properties the TZM alloy has to offer in the conditions the components of the thruster were exposed to.

Another publication was found incorporating TZM into an Arcjet thruster. Researchers Zube, Glocker, and Kurtz developed a low power, radiatively cooled Arcjet. TZM was used for the thruster housing and the injector disk [21]. Glocker and Kurtz stated that TZM was implemented because of its thermal properties and it is easier to machine than Tungsten.

Tungsten is another refractory metal used in aerospace components. Tungsten has the highest melting point of all refractory metals; however, it is very difficult to machine, print, and its high thermo-conductivity often times leads to cracking during printing [22]. Glocker and Kurtz indicated that not only is TZM capable of being used in components similar to what will be created in this effort, but also some of the benefits of using it over a different refractory metal.

Another instance in which TZM has previously been incorporated in aerospace is for a patent filed by Robert J. Cavalleri and Thomas A. Olden. Cavalleri and Olden made a solid fuel rocket motor using pellets and bulk solid propellants [23].

Cavalleri and Olden developed a pellet retainer that was positioned to retain the fuel pellets within the casing. Exhaust gases pass through the pellet retainer to the nozzle without allowing fuel pellets

to leave the device before combusting. This device incorporated TZM specifically in a way so that it would be directly exposed to the combustion gases of the pellets. This source iterated that again TZM is appropriate for use in smaller type thrust devices, as well as can be exposed to outright combustion in certain configurations.

After seeing these examples, among others, it was concluded that there was enough supporting evidence of the use of TZM in aerospace. However, keep in mind that these were instances of TZM being machined for the components. In this effort, TZM will be AM. There is little available research on the effects printing powdered TZM has on its thermal and mechanical properties compared to solid TZM. The next step in the research was to see if TZM would be fit for AM. This is discussed further in the following section.

2.2 Preliminary Investigations using TZM for AM

Laser-based powder bed fusion (L-PBF) was the technique of choice to additively manufacture the TZM for this research. The bottom-to-top nature AM offers is attractive due to the freedom of design complexity and conservation of materials [24]. Although L-PBF is believed to be a reliable technology to use, there are some problems with establishing printing parameters.

Currently, most publications regarding L-PBF do not focus on establishing a standard process to optimize printing parameters, however, research is focused on particular alloys as they are printed on specific machines [25]. This means that a general, standard process of selecting initial printing parameters does not exist. Instead, expensive, empirical "guess-and-check" type operations are conducted that may or may not give acceptable print results. [25-26].

The research team began searching for publications where TZM had been AM. It was believed that by doing this, initial parametrization could be expedited. It was discovered that literature on L-PBF with TZM is scarce. The research team then began to broaden the scope of the literature review by looking for pure Molybdenum AM publications. Due to TZM being over ninety-nine percent Molybdenum, it was considered acceptable to reference these sources.

A study conducted by Dr. Faidel titled "*Investigation of the Selective Laser Melting Process with Molybdenum Powder*" was selected for reference due to similarities in initial geometries (cubes) and PBF machines available at UTEP. In this study, Faidel performed multiple prints of cubes, honing in on print parameters such as maximum spot diameter, spot velocity, and laser power. Faidel was measuring and recording surface roughness and print density of the specimen while adjusting the print parameters [27]. Following is a table from Faidel's research depicting the parameters used for experimentation [27].

Table 4: Printing Parameters Used in Faidel Study

No.	P_L [W]	$2\omega_0$ [µm]	v_L [mm/s]	d_s [µm]	y_s [µm]	E_V [J/mm^3]
1	200	50	556	45	10	200
2	200	50	556	45	30	400
3	200	50	278	45	10	400
5	200	50	278	45	20	533
6	200	50	139	45	20	1066
7	200	50	556	25	10	360
8	200	50	556	25	30	720
9	200	50	556	25	20	480
19	200	50	1112	45	20	133
20	200	50	1112	25	20	240
21	200	50	2224	25	20	120
23	200	50	4448	25	20	60

The parameters used in the Faidel study aided the UTEP effort in that it validated that Molybdenum powders could be attempted to be printed using L-PBF with machines comparable to those available at the University. However, Faidel's specimen consistently had undesirable surface roughness and porosity values. Also, the highest specimen density achieved compared to solid TZM was slightly above eighty-five percent. Although Faidel's paper is useful for a preliminary investigation, it was desired to improve density, surface roughness, and porosity for the UTEP study. Following is a figure of a bar graph depicting the density values achieved for Faidel's specimen [24].

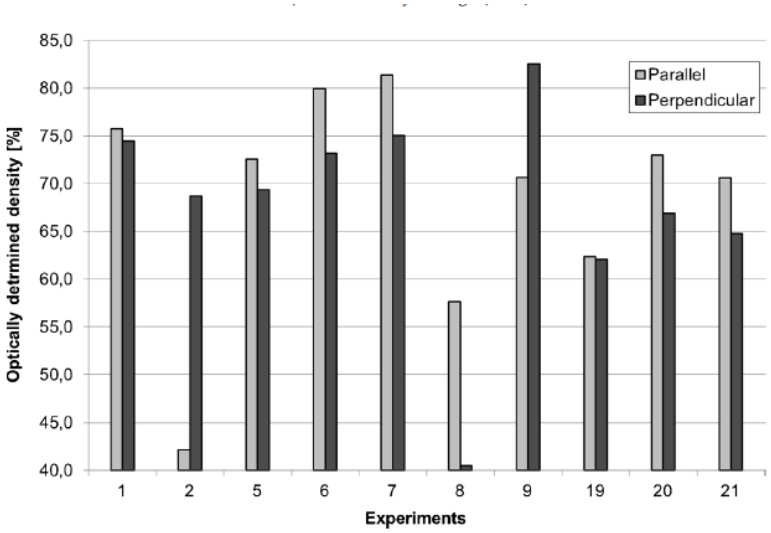

Figure 2: Density Values Found in Faidel Study

After verification that Molybdenum powders could be printed with parameters possible with UTEP machines, the research team wanted to validate a way to begin methodically assessing the printability of TZM. An expensive trial and error type investigation was not an option for this research. After referencing Faidel's study, a more empirical approach was taken so as to hone in on print parameters for TZM. The following section discusses this in more detail.

2.3 Theoretical/Empirical Investigation - Introduction

As stated in section 2.2, a standard method for establishing confidence in material printability does not exist. After reviewing the Faidel study, the research team began to conduct a theoretical/empirical study regarding TZM. The study was conducted to cover optical processability, thermal processability and required volume energy density (VED) to melt the material. The study was theoretical and empirical in nature because it combined the aspects of theoretical processability values with information form previously printed alloys to indicate the parameters needed to print TZM.

The research team used a paper titled "*Development of Laser-Based Powder Bed Fusion Process Parameters and Scanning Strategy for New Metal Alloy Grades: A Holistic Method Formulation*" conducted by Bassoli and team to aid in parameter development [28]. The Bassoli study discussed the need for an accepted method for parameter selection in L-PBF AM. By comparing mechanical and physical properties of alloys that are known to be printable, the Bassoli study establishes a method of evaluating a new alloy for possible printing. The following is the method used in this research effort adapted from the Bassoli study.

2.4 Theoretical/Empirical Investigation – Optical Processability

The first processability factor to investigate is the optical/reflectivity characteristics of the powder. Reflectivity is important from a processability standpoint for two reasons; it depicts the powder's ability to absorb enough energy from the laser to melt, and if major reflection occurs, it indicates possibilities of the reflection damaging the laser. Highly reflective materials such as Aluminum-based alloys or Copper have the potential to damage AM equipment [29].

According to Bassoli and citation source [29], the reflectivity value of the powder (R_{powder}) can be assumed to be seventy percent of the solid version of the alloy (R_{bulk}). In order for the powder to be considered optically possessable, R_{bulk} cannot exceed ninety-five percent of the value of the operational wavelength of the laser. Typically, PBF lasers operate at wavelength of 1.06 micrometers (1060 nanometers), as is true with machines that were used this effort. This would mean that the R_{bulk} cannot exceed 1007 nanometers subsequentially meaning that R_{powder} should not have a value higher than 705 nanometers.

Experimentation conducted by Coblentz resulted in obtaining the reflecting power of various metals, one of which is Molybdenum [30]. Coblentz obtained the percentage of reflectivity of metals at wavelengths varying form 0.5 – 10 microns. Following is a table from the Coblentz research depicting Tungsten and Molybdenum reflectivity values [30].

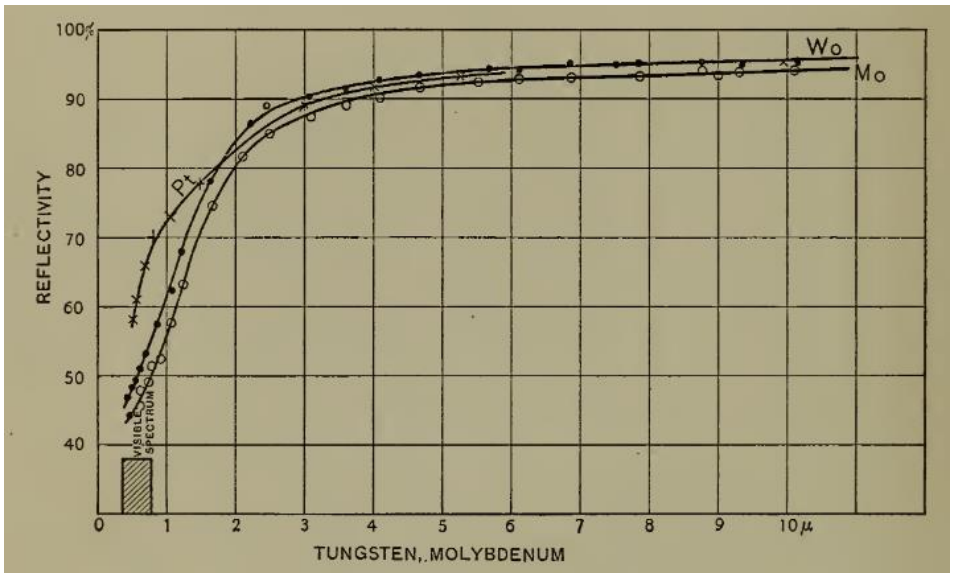

Figure 3: Reflectivity Values for Tungsten and Molybdenum from Coblentz Study

As can be seen from the figure above, solid Molybdenum possesses reflectivity values ranging from approximately sixty-five to eighty percent when subjected to light sources having wavelengths from one to two microns. This indicates that the R_{bulk} value is within the required percentages to be optically processable. There were some assumptions made in that the reflectivity values were for Molybdenum instead of TZM. Regardless, the actual TZM values for reflectivity are expected to be very similar.

There is also a theoretical way to calculate reflectivity of powdered alloys that was instituted in this effort. Specifically, the theoretical optical processability method was used to characterize R_{powder} values for other alloys and compare them to TZM. This is explained in further depth in Section 3.5.

2.5 Theoretical/Empirical Investigation - Thermal Processability

After validating the reflectivity of the powder, next was the thermal processability (TP). According to Bassoli, the TP value is used as a preliminary indicator if the alloy will be printable. In essence, it is the ratio of the materials thermo-conductivity (k) versus the linear shrinkage (l_s) the alloy is subjected to while cooling off. This linear shrinkage is calculated by multiplying the difference in the melting temperature of the alloy and the ambient environment (ΔT) with the value of the coefficient of thermal expansion of the alloy at a solid state (α).

$$l_s = \alpha \cdot \Delta T \tag{2.1}$$

Ergo, TP can be found via:

$$TP = \frac{k}{l_s} \tag{2.2}$$

For this formula, the melting temperature of TZM (2,623 degrees Celsius) compared to room temperature was used for temperature difference. If this were to result in an undesirable TP value, then the ambient temperature could be adjusted by heating the powder bed, changing the value of the temperature difference. This will be discussed in further detail in Chapter 3.

According to the Bassoli study, a higher value of TP should be indicative of a material that is easier to print, and a lower TP value means that's a material will be harder to print, from a thermal standpoint. Following is a table showing reference alloy data from the Bassoli study that are considered to be printable with their respective thermophysical and TP values.

Table 5: TP Values for Known Alloys

Thermal Processability Values for Known Alloys					
Material/Alloy	Cited Source	k (W·m-1·K-1)	α (K-1)	ΔT (K)	TP (W·m-1·K-1)
AlSi10	[31]	113	2.20E-05	570	9011.16
Ti-6Al-4V	[31]	6.7	9.20E-06	1635	445.42
Inconel 625	[32]	9.8	1.50E-05	1330	491.23
AISI316	[32]	16.2	1.62E-05	1380	724.64
Hastelloy X	[32]	9.1	1.60E-05	1335	426.03
Cu	[31]	391	1.77E-05	1060	20840.00

Essentially the TP value is a comparison between how effectively a material absorbs/relinquishes thermal energy compared to its innate characteristic to expand/retract within the range of the expected temperature the alloy will see during printing. These thermophysical values are important, because it explains how an alloy will react when rapidly heated/cooled. For example, an alloy with a low thermal conductivity will remain as a molten pool and agglomerate, however if it is susceptible to a high thermal expansion, cracks/failures could occur throughout the printed geometry [33]. The Bassoli study states, "*As a guideline, the procedure proposed here has been proven feasible for Inconel 625 but has not been verified yet for lower values of TP*," indicating that TP values higher than Inconel 625 (491.23) should be considered acceptable to print, from a thermal point of view.

There are other aspects to consider when attempting to characterize the printability of an alloy. The following section will cover volume energy density (VED), and the sub-parameters that go into finding the VED values.

2.6 Theoretical/Empirical Investigation - Volume Energy Density

VED is an often time used parameter to evaluate specimen that are manufactured by SLM [34]. By obtaining the VED, initial bulk geometries and the metrics needed to manufacture them can be determined. In simple terms, VED can be described as the required energy density needed to melt the powdered alloy during the printing process [35]. As was the case for the optical and TP values, this section adopts the steps that can be found in the Bassoli study.

VED is difficult to calculate accurately as there are several unknown variables that occur during the laser melting process. This requires there to be assumptions made during the calculations. A simplistic method of being able to find VED can be conveyed by beginning with the heat required per unit volume (*q)*. The *q* value of an alloy can be found in the following equation.

$$q = (c \cdot \Delta T + l_f) \cdot \rho_{powder} \tag{2.3}$$

In the equation above, *c* is the specific heat capacity, l_f is the specific latent heat of fusion, and ρ_{powder} is the density of the powdered alloy. In this formula, as is the case in formula (2.1), ΔT is the difference in the melting temperature of the solid alloy, and room temperature (20 °C).

Throughout the process of AM with SLM, there are energy losses experienced in the print field for a variety of reasons; reflectivity, cooling of melt pool via thermal conduction, dissipation, and many others [36-37]. These losses directly affect the printability of the alloy from a VED standpoint. In order to account for losses, an efficiency term (η) is implemented.

$$VED = \frac{q}{\eta} \tag{2.4}$$

Efficiency as found in the Bassoli study was estimated by taking into account losses due to reflection and conduction. This is a rough estimate for a L-PBF process. There are other losses that can occur. For example, interference between laser beam from dust or splattering from the melt

pool as are described in more detail in source [38]. The Bassoli method describes the most idealistic version of the L-PBF. Although not guaranteed to be completely accurate, it is helpful for the initial investigation. Following is an equation describing the η term.

$$\eta = (1 - R_{powder}) \cdot (1 - k_{rel}) \cdot \eta^* \tag{2.5}$$

In the equation above, R_{powder} and k_{rel} are the reflectivity and relative thermal conductivity of the powdered version of the alloy. The η^* term is imposed upon the equation in order to take into account any other losses that were neglected. The Bassoli study assumes a first estimate of $\eta^*$to be roughly twenty percent, however this may vary depending on a number of variables respective to alloy and machine used.

The k_{rel} value can be obtained by finding the ratio of the thermal conductivity of the powder versus the thermal conductivity of silver, as seen in the equation below.

$$k_{rel} = \frac{k_{powder}}{k_{Ag}} \tag{2.6}$$

Keep in mind that the thermal conductivity of the powder is not the same as the thermal conductivity of the solid version of the alloy. In order to obtain the correct value for thermal conductivity, the "*Rule of Mixtures"* as it is applied to material sciences is used. This allows for upper and lower estimates for composite like materials for properties such as elastic modulus, tensile strength, and in this case, thermal conductivity [39-40]. This can be seen in the following equation.

$$E_c = f \cdot E_f + (1 - f) \cdot E_m \tag{2.7}$$

E_c is typically the value for elastic modulus of a composite while E_f and E_m are the elastic modulus for the fibers and matrix, respectively for a composite. The f term is the volume fraction of the fibers. Because this equation can be adapted for several properties, thermal conductivity can be found, and instead of a composite made up of fibers and a matrix, the equation will describe the volume fractions of the powder and gas present in the build chamber. This adapted equation is as follows.

$$k_{powder} = k_{metal} \cdot V_{metal} + k_{gas} \cdot (1 - V_{metal}) \tag{2.8}$$

In the previous equation, k_{metal} is the thermal conductivity of the alloy in its solid form and k_{gas} is the thermal conductivity of the gas present in the build chamber, (in this research, it is Ultra-High-Purity-Argon). For the Bassoli study, it was assumed that V_{metal} is fifty percent of the powder layer, reducing equation (2.8) to the following form.

$$k_{powder} = 0.5 \cdot (k_{metal} + k_{gas}) \tag{2.9}$$

When summing the thermal conductivities of gases and solids, the thermal conductivity of the gas can be neglected. This is because solids have a thermal conductivity that is up to four orders of magnitude larger than a gas [41]. The thermal conductivity of Argon at 300 K is 0.018 W/m-K. Under the same conditions, Molybdenum has a thermal conductivity of 138 W/m-K. This reduces equation (2.9) to the following.

$$k_{powder} = 0.5 \cdot k_{metal} \tag{2.10}$$

Taking all of the previous equations into consideration, an expanded equation for the VED is as follows.

$$VED = \frac{q}{\eta} = \frac{(c \cdot \Delta T + l_f) \cdot \rho_{powder}}{0.2 \cdot (1 - R_{powder}) \cdot (1 - \frac{0.5 \cdot k_{metal}}{k_{Ag}})} \quad (2.11)$$

An important concept to note is that during the line scanning of the printing process, one side of the scan path will overlap solidified material, while the other will be in contact with the unmeted powder [42]. Equation (2.11) only takes into account the thermal conductivity of the powder, making it a calculation describing the lowest possible condition for thermal conductivity.

To be completely accurate, a second method would need to be implemented in order to account for the two different conditions, however for this research, equation (2.11) is considered to be enough for preliminary parameter investigations.

The following equation expresses the VED obtained in equation (2.11) from the machine's laser point of view.

$$VED = \frac{P}{L \cdot h \cdot v} \quad (2.12)$$

In equation (2.12), *P* is the power of the laser, *L* is the layer thickness, *h* is hatch distance, and *v* is equal to the laser scan speed. Equation (2.11) can be used as an initial process to approximate the VED. Equation (2.12) can be used systematically before and during the printing process to identify the ideal parameters from the laser. Both equations are used in this research to assign parameters of the laser during printing.

It was the strategy of this research to use equation (2.12) before and during printing, varying the parameters of the laser. Systematic changes to the printing demonstrate the effectiveness of higher or lower VED values. For example, lower VED values result in a lower temperature of the melt pool and ultimately a higher cooling rate [43]. Higher values for VED result in better metallurgical

bonds but can have higher thermal stresses and production of spherical pores [44]. The strategy of this research was to estimate a higher and lower boundary for the VED value, thus illustrating what the laser parameters could be, (this is discussed in further detail in chapter 3).

2.7 Summation of Background and Theory Section

When investigating a new alloy for the AM process, it is difficult to conduct the initial parametrization. There is ample literature on alloys printed with specific machines in the past. Typically, these alloys have been subjected to numerous guess and check type studies that have established their printability as well as parametrization.

Because an expensive guess and check style methodology was not an option for this research, alternative efforts were implemented. First the alloy was investigated for use in aerospace. Next, studies of similar Molybdenum powders were investigated to give confidence in the use of the TZM alloy for AM. Next, a model adapted by the Bassoli study was implemented so as to theoretically/empirically investigate the printability of the TZM alloy. While investigating processability, initial parameters were established based on comparison to similar alloys, literature review, and experience form the W. M. KECK Center. This is discussed further in the next chapter.

In this research the primary indicator for a successful print was the resultant density of the specimen compared to the solid density of TZM. A specimen is considered to be printed successfully if it has a percent value that is higher than ninety percent the density of solid TZM. Further honing will be done in the future to reach the target density percentage of %99.5. The research conducted solely printed specimen directly to the build plate with no support structures. Support structures and over-hanging geometries will be investigated during the next phase of this effort.

The following chapter will describe the methodologies of the study beginning with comparing the material properties of TZM to other printable alloys and ending with the plan used to print/analyze the TZM specimen.

Chapter 3: Methodologies

This section describes the methodologies implemented to conduct research on the TZM alloy. As was discussed in Chapter 2, TZM was subjected to theoretical/empirical investigation, and the properties of the alloy were compared to other known printable materials. This strategy was executed because it was believed that it would assist in circumventing an expensive guess and check style of research.

This chapter begins by discussing original plans in the effort that were amended once a deeper understanding of the difficulty of printing the TZM alloy would be. After the preliminary print plan, powder selection and machine selection are discussed. The amount of powder purchased was done so in accordance to the preliminary print plan. Changes in machine choice, expectations from initial printing, and powder on hand led to the development of the adapted print plan. Also discussed in this section are comparisons of thermal, mechanical, and empirically found values as discussed in Chapter 2 between TZM and other printable alloys.

3.1 Preliminary Print Plan

This section covers the preliminary print plan of the initial phase of this research. At this time during the effort, funding was being supplied by Valley Tech Systems (VTS). VTS desired to AM a small thruster housing out of TZM. The initial plan through VTS was to begin by printing 0.5-inch cubes to establish printing parameters of the alloy. Following would be specimen that could be tensile tested. The values from the tensile testing would be compared to values obtained from solid TZM. After receiving tensile data that was satisfactory, the thruster housing would be printed for VTS. Following are images of the cubes, tensile specimen, and thruster housings.

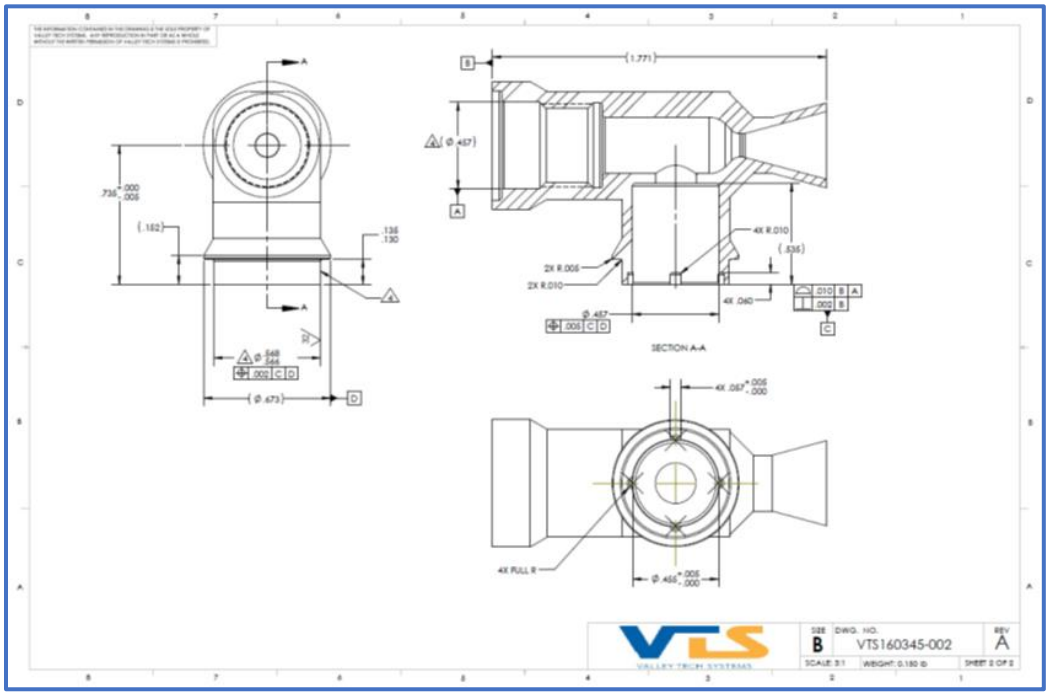

Figure 4:VTS - TZM Thruster Housing (VTS160345-002)

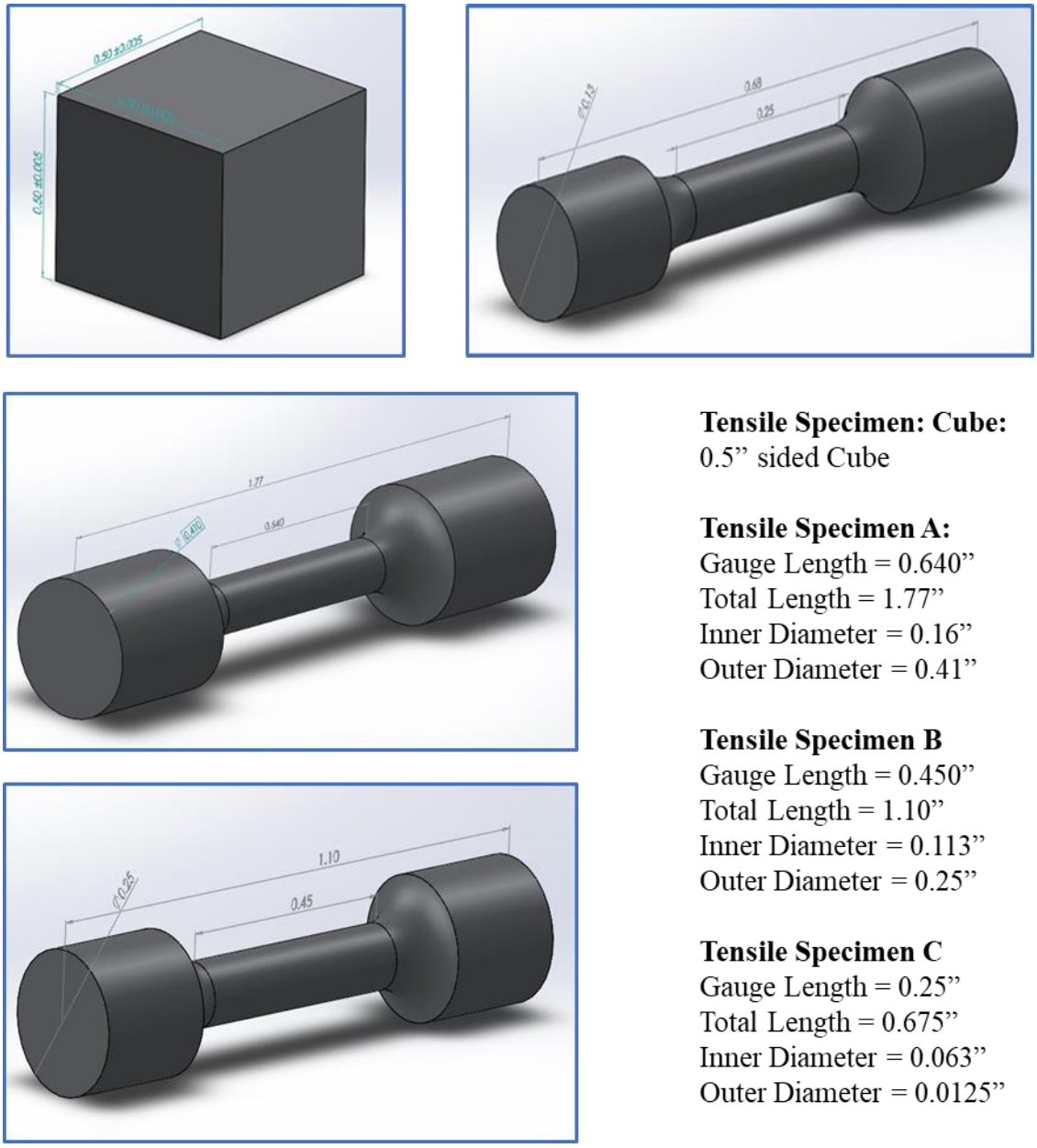

Tensile Specimen: Cube:
0.5" sided Cube

Tensile Specimen A:
Gauge Length = 0.640"
Total Length = 1.77"
Inner Diameter = 0.16"
Outer Diameter = 0.41"

Tensile Specimen B
Gauge Length = 0.450"
Total Length = 1.10"
Inner Diameter = 0.113"
Outer Diameter = 0.25"

Tensile Specimen C
Gauge Length = 0.25"
Total Length = 0.675"
Inner Diameter = 0.063"
Outer Diameter = 0.0125"

Figure 5: Images and Details of Tensile Cube and Specimen for Preliminary Print Plan

In the figure above, the Tensile Cube is depicted in the upper left, Tensile Specimen C is on the upper right, Tensile Specimen A is in the middle, and Tensile Specimen B is on the bottom.

Cubes are a typical preliminary geometry to begin with in AM as can be seen in the Faidel study. Tensile specimen A, B, and C were designed in accordance to the ASTM E8 standard. This was done because of the similar dimensions between the standard and the thruster housing. These

designs can be adjusted slightly so the specimen can be processed after manufacturing for tensile testing.

The original print plan was composed of three series, beginning with the cubed specimen and ending with the thruster housings. After learning more about TZM and discovering how difficult it would be to print, the plan was adapted. This will be covered in Section 3.4.

This section was included in this thesis, because the amount of powder that was ordered was in accordance to preliminary print plan. The preliminary print plan series were proposed to be as follows.

Print Series 1: This series was to be the first printing done in the effort. During this series three of the Tensile Cubes were to be printed as well as two of Tensile Specimen A, B, and C. The specimens were to be subjected to various testing in order to obtain information regarding the printing.

Print Series 2: By Print Series 2, it was expected for there to be an in-depth awareness of the printing parameters as learned from Print Series 1. This would allow for the team to attempt to print a thruster housing as well as two of Tensile Specimen A components for the X, Y, and Z directions of the housing.

Print Series 3: Print Series 3 would print the same components as Print Series 2. This would allow for any adjustments to be made as needed when printing the housing and the required tensile specimen.

3.2 Purchasing TZM Powder

Pure casted TZM Molybdenum is 99.40% molybdenum, 0.50% titanium, 0.08% zirconium, and 0.02% carbon. Powdered TZM molybdenum is offered by most vendors in purity ranging from 2N to 5N purity (99.0% to 99.999%). The differing purity has potential to affect the mechanical properties of prints, as well as printability [44]. It was up to VTS to decide which percentage would be purchased as they do vary drastically in cost per kilogram.

Originally, the EOS M290 was the AM machine of choice for this effort. After conducting further research, a different machine was selected as will be discussed in Section 3.3. However, the amount of powder for purchase was decided by using the dimensions of the EOS M290 build platform.

To calculate the needed powder mass, first volume was found using the area of the build plate multiplied by the tallest object to be printed, (the thruster housing). Multiplying this value by the total number of prints, including cubes and tensile specimen, gave the total volume of powder needed.

Powder not used in PBF printers during a print can be recycled. The percent of powder recyclable helps decrease the total mass of powder needed to be purchased. The calculations were adjusted for an assumed recyclability of ninety percent [43]. Also calculated was the necessary mass of powder if zero percent of the powder was recycled. This was done so as to give VTS a range of required powder amounts to purchase. Following is a table depicting the required powder calculations.

Table 6: Overview of Machine and Specimen Characteristics

Known Information:	**Value**	**Units**
EOS M290 Build Volume (9.85 x 9.85 x 12.8 in)	1240	in^3
EOS Build Plate Area (9.85 x 9.85 in)	97.02	in^2
Tensile Specimen Dimensions	ASTM E8 (proportionally)	
Thruster housing dimensions (VTS Drawing)	Approximated	
Thruster housing height	1.771	in
Density of TZM Molybdenum based on VTS's specs	0.37	lb/in^3
Tensile specimen length	1.771	in
Tensile specimen outer diameter	0.41	in
Cube specimen (0.5 x 0.5 x 0.5 in)	0.125	in^3
Assumptions:		
Number of tensile specimens to be printed (3 per X, Y, Z orientation)	9	
Number of thruster housings to be printed	2	
Volume of tensile specimens estimated as a straight cylinder	Volume of each specimen varies	
Volume of thruster housing estimated as a solid block, coinciding the thruster's outer dimensions	1.35	in^3
Density of printed TZM to Solid TZM assumed 1:1	0.37	lb/in^3
Additional powder for trial runs	5	kg
Total build height rounded up to the nearest inch	2	in

Component	**Mass**	**Unit**	**Outer Diameter**	**Length**	**Unit**
T. Specimen A	0.03800	kg	0.41	1.771	in
T. Specimen B	0.00905	kg	0.25	1.10	in
T. Specimen C	0.00139	kg	0.125	0.675	in
0.5 in Cube	0.02180	kg			

Table 7: Powder Required for Prints

Powder Required for prints			
Quantity	*Component*	*Mass*	*Units*
Print Series 1			
2	T. Specimen A	0.076	Kg
2	T. Specimen B	0.018100047	Kg
2	T. Specimen C	0.002778	Kg
3	0.5 in cube	0.0654	kg
Print Series 2			
1	Thruster Housing	0.2262735	Kg
3	T. Specimen A	0.228	Kg
Recycled powder if reused from first print		29.10846191	Kg
Additional powder needed to complete print 2		3.414582487	Kg
Print Series 3			

1	Thruster Housing	0.2262735	Kg
3	T. Specimen A	0.228	Kg
Recycled powder if reused from first print		28.86189381	Kg
Additional powder needed to complete print 3		3.66115059	Kg

Table 8: Total Powder Required

Total Powder needed		
With 90% recyclability	39.59877748	Kg
Rounded up with +5 kgs	~45	Kg
With 0% recyclability	97.6967205	Kg
Rounded up	~100	Kg

It was concluded that forty-five kilograms of TZM would be purchased for the effort. After calculating the required powder, next was to decide a purity and a vendor. The team began researching several vendors and made a list of five that would be able to provide the powder. They are as follows.

- READE Advanced Materials
- American Elements
- H. C. Stark
- Eutectix
- Global Tungsten Products

VTS ultimately decided the vendor, amount, and purity of the TZM powder. American Elements was selected, because it was the only vendor found that could supply the powder within the time constraints. Other vendors were nonresponsive, or were not able to provide the alloy. The purity and amount were believed to have been decided due to cost constraints.

3.3 Machine Selection

Printing was done by the W. M. KECK Center on the UTEP campus. The KECK Center has several different platforms to offer in the AM fields. Originally the research team was interested in using the EOS M290 machine. This was because the EOS has a smaller build space, meaning that less powder would need to be used for printing in the machine. Also, the EOS has preheating capabilities for up to 200 degrees Celsius, which was later found to be too low of a capability for the TZM alloy. Following is a table containing the specifications of the EOS machine.

Table 9: EOS Machine Specifications

EOS M290 Technical Specifications	
Build Space	250mm X 250mm X 250mm
Laser Power	400W
Optics Configuration/ spot size	Highspeed scanner/ 100 µm
Preheating Temperature	200 C
Inert gas Type	Nitrogen

After learning more about the TZM alloy, it was discovered that the EOS may not be the proper machine for the job. The EOS is a decent machine when printing known alloys that have lower melting points than TZM. However, for research purposes, the team needed a machine that had more versatility in order to address the wide range of unknown parameters.

The KECK Center is one of only a few institutions that has an Aconity One AM machine. The Aconity machine was originally designed by its manufacturer for research purposes. This machine is equipped to control a wide variety of processing parameters resulting in a more versatile system compared to the EOS. Some of these parameters, such as laser power and scan

speed, can even be adjusted mid-print. Following is a table depicting the specifications of the Aconity machine.

Table 10: Aconity Machine Specifications

Aconity One Technical Specifications	
Build Space	400mm diameter 400 mm height
Laser power	Single Mode Fiber 400W/1000W
Optics Configuration/ spot size	3D Scanning/ 80-500 µm
Preheating temperature	1000 C
Inert gas type/ Pressure	Argon/Nitrogen (max 6 bar)
Residual Oxygen Content	<500 ppm

The main driver behind making the switch to the Aconity is that is possess much higher preheating temperature capabilities than the EOS. This is important because some of the experienced personnel form the KECK Center were very concerned with the alloy cracking during printing. This higher preheating capability shortens the gap between the melting temperature of the TZM and the ambient environment resulting in less thermal stresses.

The research team ultimately decided to go with the Aconity One because it is a more flexible machine than the EOS. Because of its capabilities, the Aconity seemed more suitable for research. At this point in the effort, it was decided by the team to draft a new print plan. The original plan provided primarily by VTS was considered to be too earnest. As more was learned about the alloy, it was discovered that it could prove difficult to print. This along with the decision to use a different machine resulted in the need of an adapted print strategy. The adapted print plan for this study is discussed in the following section.

3.4 Adapted Print Plan

The starting point in the preliminary print plan was going to be half inch cubes. The preliminary print plan would have ended with two thruster housings that could be high pressure tested. Due to lack of published literature on AM TZM, and the amount of unknown printing parameters and expected results, it was decided to revise expectations of initial printing.

The adapted print plan would focus exclusively on preliminary geometries. The geometries selected were seven-millimeter diameter cylinders that are ten millimeters in height. The cylinders were requested by VTS rather than cubes. This was because it was believed that their machinist could do more investigative post processing with cylinders versus the cubes.

The adapted print plan was made up of three print series. The first print series would print twenty-one cylinders with a wide range of parameters. Post printing analysis for surface finish, density, and image processing would indicate which cylinders were printed the best. From there, the printing parameters would be adjusted, and a new series of cylinders printed. This would continue until cylinders could be continually printed with acceptable geometry percentages (above ninety percent of TZM). After that, depending on the amount of powder that is left, larger geometries and tensile specimen could be printed. Following is an image depicting the Adapted Print Plan.

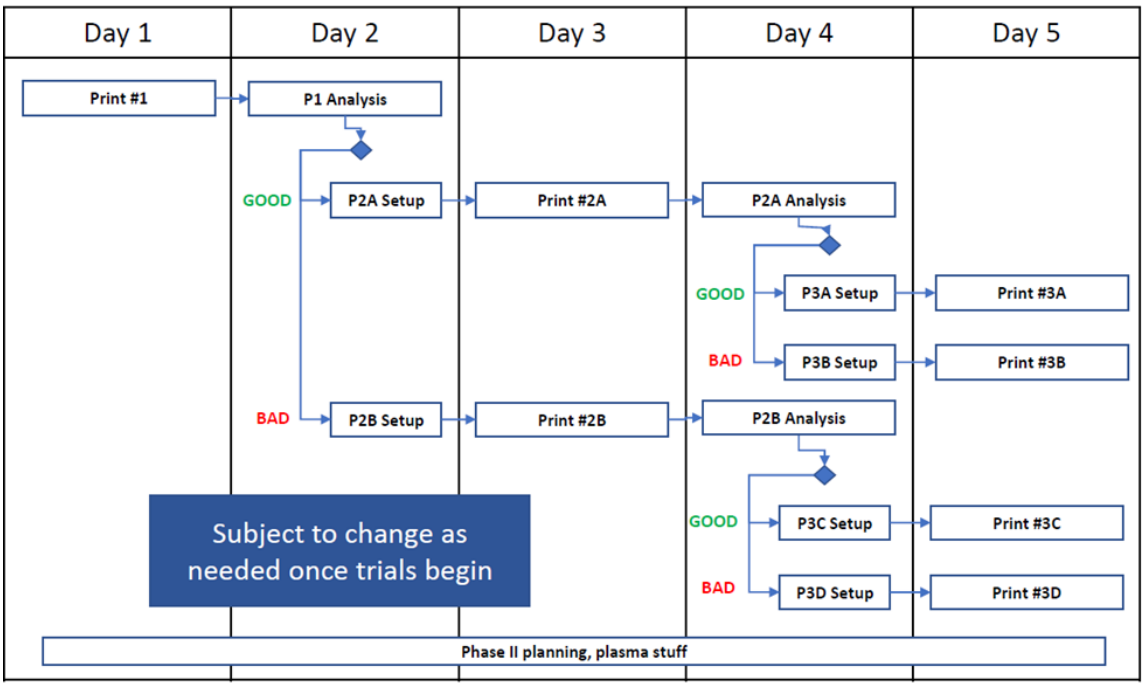

Figure 6 : Flow Chart of Adpated Print Plan

As can be seen in the chart above, the adapted print series was designated over a five-day print period. This was done in accordance to the amount of powder that was purchased. The plan was left flexible during the printing because there is so much that is unknown about additively manufacturing the alloy. It was the goal of this amended print plan to find out as much information as possible about using the L-PBF with TZM.

Referring to Chapter 2, it can be see that from the equations implemented to find VED, printing parameters for the laser and print bed can be implemented. Using the knowledge from experience of the KECK center, the cumulation of information found on the alloy, the following image shows charts of VED values with varying printing parameters.

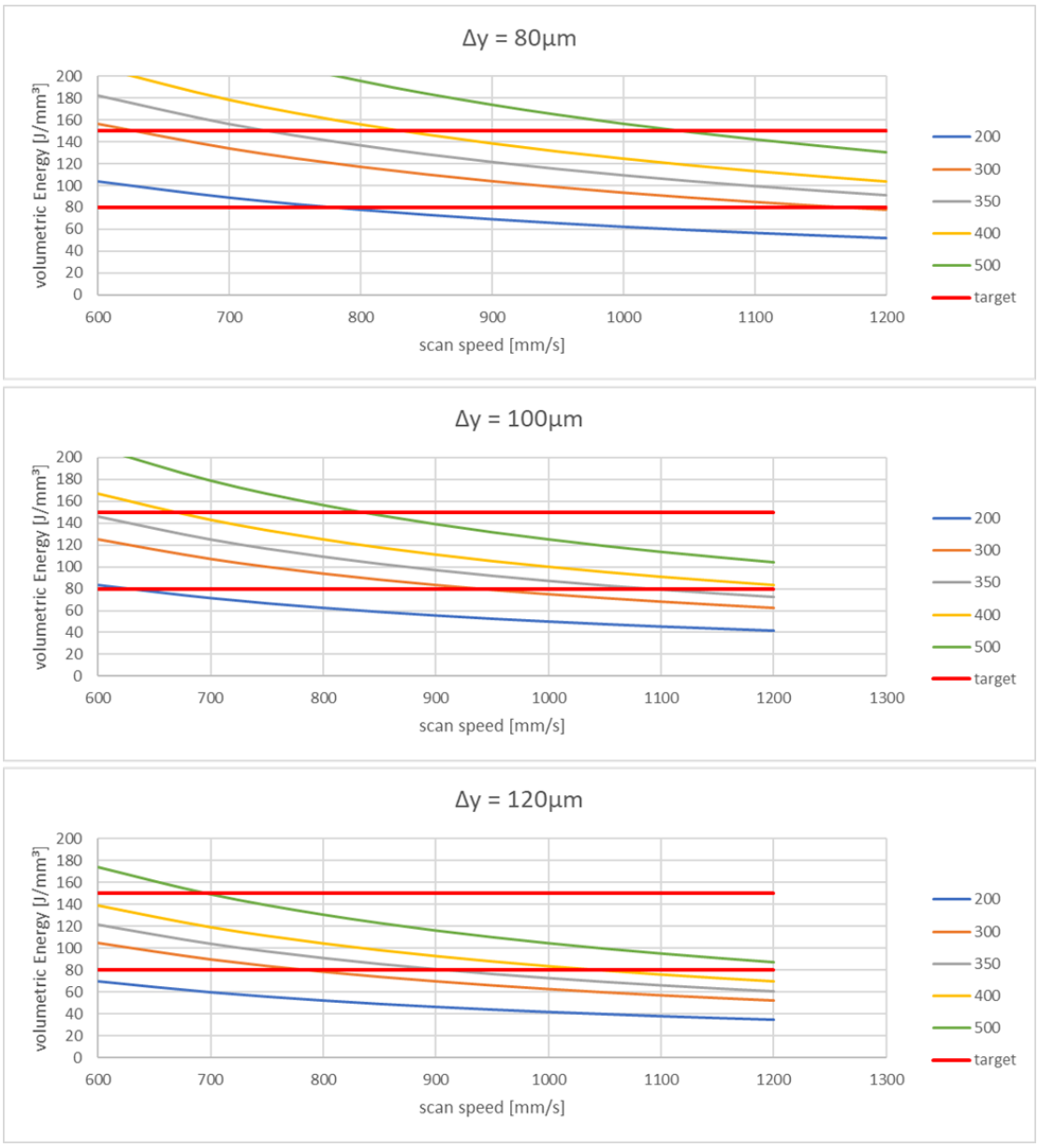

Figure 7: VED Values with Differing Print Parameters

The graphs above depict trends of VED values for altering values of the laser parameters such as power of the laser, the hatch distance, and the laser scan speed. Each graph is formatted to a specific hatch distance denoted here as Δy. The calculated value of VED for TZM is roughly 80 j/mm3. In the graphs above, this value is representative of a lower boundary target value for VED. The higher boundary target for the VED is 150 j/mm3. This strategy implemented allows

for altering of parameters before printing giving an idea to the researchers what changes may occur when changing laser/print parameter values. Parameter altering could occur as long as the resulting VED values fit between or close the two boundaries. The specific print parameters assigned to each print geometry is given in Results portion of the thesis (Chapter 4).

3.5 TZM and Molybdenum Comparison to other Alloys

Along with the adapted print plan comparisons between Molybdenum/TZM and other printable alloys were made and recorded. The purpose of this was to create a bank of information of L-PBF alloys. After a print of TZM was completed, the material data from the other alloys could be compared to that of TZM so as to explain the results and help to make adjustments to the printing parameters. The alloy characteristics that were found were mechanical/physical information, thermal characteristics, reflectivity, TP, and VED values.

As mentioned in Chapter 2, reflectivity is an important parameter because it describes the amount of energy a powder will either absorb or reflect. The lower the reflectivity value, the more energy that is absorbed, increasing the efficiency of the printing process. A method adapted from a paper titled "*Metal powder absorptivity: Modeling and Experiment*" by C.D. Boley was used in this effort to assign reflectivity values for various alloys [45].

Boley's method can be used for three different powder distribution arrangements; hexagonal, gaussian, and bimodal. For this effort, the gaussian method was used because of the characteristics of the TZM powder as is discussed in Section 4.1. Gaussian methods are used for powders having higher porosity, lower density, and particulate sizes at the maximum diameter (45 μm), the average (30μm), and the minimum particle size (15μm).

The equation to calculate the gaussian powder absorptivity (A_{pow}) is as follows.

$$A_{pow} = 0.0413 + 2.89 \cdot A_n - 5.36 \cdot {A_n}^2 + 4.50 \cdot {A_n}^3 \quad (3.1)$$

The variable "An" is the flat surface absorptivity. The equation to calculate flat surface absorptivity can be approximated using the following equation.

$$A_n(0) = 4 \cdot \xi \quad (3.2)$$

The variable ξ is representative of the surface impedance and can be calculated using the materials refractive index and extinction coefficient at the designated wavelength (one micron). Surface impedance can be found in the following equation.

$$\xi = R_e\left(\frac{1}{n}\right) = \frac{n_r}{{n_r}^2 + {n_i}^2} \tag{3.3}$$

Applying the above equations for alloys that have been printed in the KECK center previously or found through literature review produced the following table.

Table 11: Reflectivity Data Values for Known Alloys

Material	Refractive index	Extinction Coefficient	Surface Impedance	Flat Surface Absorption	Reflectivity Value	Absorption	Reflectivity
TZM	2.53	4.00	0.11	0.452	0.548	0.711	0.289
Molybdenum	2.53	4.00	0.11	0.452	0.548	0.711	0.289
Ti6242	3.37	3.98	0.12	0.496	0.504	0.743	0.257
Al6061	1.43	9.5	0.02	0.062	0.938	0.240	0.760
AlSi10Mg	1.43	9.5	0.02	0.062	0.938	0.240	0.760
Ti-6Al-4V	3.37	3.98	0.12	0.496	0.504	0.743	0.257
Inc 625	3.45	5.1	0.09	0.364	0.636	0.641	0.359
Cu	0.33	6.6	0.01	0.030	0.970	0.173	0.827

These values aided in assessing the reflectivity characteristics of TZM indicating that the powder has an acceptable reflectivity value for the threshold of this research.

Next it was desired to collect and display property characteristics for known alloys and compare them to TZM. This can be seen in the table below.

Table 12: Property Comparison Table for Known Alloys

Property Comparison Table for Known Alloys											
Material/Alloy Propety	Unit	TZM	Mo	Ti6242	Al6061	AlSi10Mg	Ti-6Al-4V	Inc 625	316ss	Hastelloy C-276	Cu
Thermal conductivity Bulk	W*m^-1-K^-1	126	138	7.1	167	124	6.7	9.7	16.3	10.5	385
Thermal Conductivity Powder	W*m^-1-K^-1	63	69	3.55	83.5	62	3.35	4.85	8.15	5.25	192.5
Thermal Expansion Coeff	1/k	4.90E-06	4.90E-06	8.10E-06	2.36E-05	2.07E-05	8.60E-06	1.28E-05	1.60E-05	1.12E-05	1.64E-05
Melting Temperature	k	2896	2883	1973	925	843	1933	1623	1673	1644	1356
Latent Heat of Fusion	J/kg	293000	289000	419000	398000	544870	370000	330000	255727	339547	204800
Density	kg/mm^3	1.02E-05	1.20E-05	4.54E-06	2.70E-06	2.67E-06	4.43E-06	8.44E-06	8.00E-06	8.89E-06	7.76E-06
Specific Heat Capacity	J/(Kg*K)	250	255	460	896	920	526.3	410	500	427	385
Tensile Strength	Mpa	965	515	1010	310	370	900	990	550	800	210
Yeild Strength	Mpa	860	415	990	276	200	830	580	240	407	33.3
Modulus of Elasticity	Gpa	325	330	120	68.9	65	113.8	207.5	193	206	110

The purpose of doing this was so as to have material data on other alloys that are known in the L-PBF community. After printing during post-processing testing and analysis, this information could be referenced and used to determine the validity of TZM prints and test results. The same logic applies for the following tables covering TP and VED values.

Table 13: Thermal Processability Values

Material	Thermal Processability (Wm-1K-1)
TZM	9886
Molybdenum	10882
Ti6242	522
Al6061	11232
AlSi10Mg	10942
Ti-6Al-4V	476
Inc 625	571
AlSi316	739
Hastelloy C-276	695
Cu	22126

Table 14:VED Values for Known Alloys

Material	Krel	Rpowder	η*	VED J/mm^3
TZM	0.155172	0.28898	0.2	80.08
Molybdenum	0.169951	0.28898	0.2	96.47
Ti6242	0.008744	0.256685	0.15	48.92
Al6061	0.205665	0.760069	0.2	68.18
AlSi10Mg	0.152709	0.760069	0.2	68.89
Ti-6Al-4V	0.008251	0.256685	0.13	56.95
Inc 625	0.011946	0.358502	0.2	58.22
AlSi316	0.020074	0.637	0.2	106.23
Hastelloy C-276	0.012931	0.476	0.2	78.68
Cu	0.474138	0.82672	0.2	261.14

After completing the characteristic investigations, it was believed by the research time that it was time to print. With all of the information from the background literature reviews, implementing a methodology for parameter assessment from the Bassoli study, constructing an adapted print plan, and investigating other alloys, the team readied for the print series. The results of the print series are covered in the next chapter.

Chapter 4: Results

This chapter covers the results from the Adapted Print Plan. It begins by displaying the results from a preliminary powder analysis. The powder analysis was conducted because the state of the powder dictates the threshold for printing results. As can be seen in Section 3.5 (reflectivity equations) and throughout Chapter 2, particulate size, shape, and morphology are very important for designating parameters and establishing processability values.

After the powder analysis, results from the printing are displayed. The researchers were disappointed in that only one print series was conducted. The results from the powder analysis were disheartening and it was concluded after the first print, better results are not feasible. As American Elements was found to be the only vendor that can currently supply the powder, the effort was put on hold until more acceptable powder could be procured. The following sections explain these subjects in detail.

4.1 TZM and Molybdenum Comparison to other Alloys

In order to conduct a thorough investigation for the use of TZM in AM, the powder purchased was subjected to powder characterization analysis. This was done to verify that the individual particulates of the powder have an acceptable shape and size, as well as proper alloying content. Another factor that is important is tap density. Tap density is directly related to particulate morphology and gives insight to the printability of the powder.

For the preliminary analysis there were three different methods used to investigate the powder:

- Initial Visual Inspection
- Powder Imaging Analysis
- Tap Density Measurements

Initial Visual Inspection: The composition of the powder purchased from American Elements was advertised as follows.

- Ti: 0.48% - 0.55%
- Zr: 0.08% - 0.12%
- C: 0.02% - 0.04%
- Mo: Balance

American Elements stated that the powder was produced by gas atomization. Gas atomization was the desired route of manufacturing the powder because it creates spherical particulates that pack and flow well during the printing process. Upon arrival at UTEP, the powder packaging was opened and the powder was visually inspected. Following are images depicting this.

Figure 8:Depiction of Powder Packaging After Arrival

It was noted by KECK center personnel that the packaging of the powder was atypical. Typically powder as such would be in cannisters versus vacuum sealed packaging. It was also noted that one of the packages had been opened indicating that a sample had been taken by American Elements for post processing analysis.

Powder Imaging Analysis: After the visual inspection of the packaging, a small sample of the powder was taken (15 mL) in order to perform the rest of the investigations. The first analyzer used on the powder was a Camsizer X2. The Camsizer is a digital imaging processing unit that utilizes two digital cameras to analyze small particles. The dispersed particles pass by LED light sources and two cameras with different resolutions capture images of particles of differing sizes. The Camsizer is coupled with an imaging software that portrays the size and shape of the particulates. This analysis showed good results in that particulates appeared spherical and were

relatively the correct size for printing (15-45 microns). This is more of a general analysis for the powder.

The next step was to use Scanning Electron Microscopy (SEM) to capture images of the powder. This imaging gives in depth, detailed images of the particulates of the powder on the micron scale. Following are the images of the TZM powder that were captured.

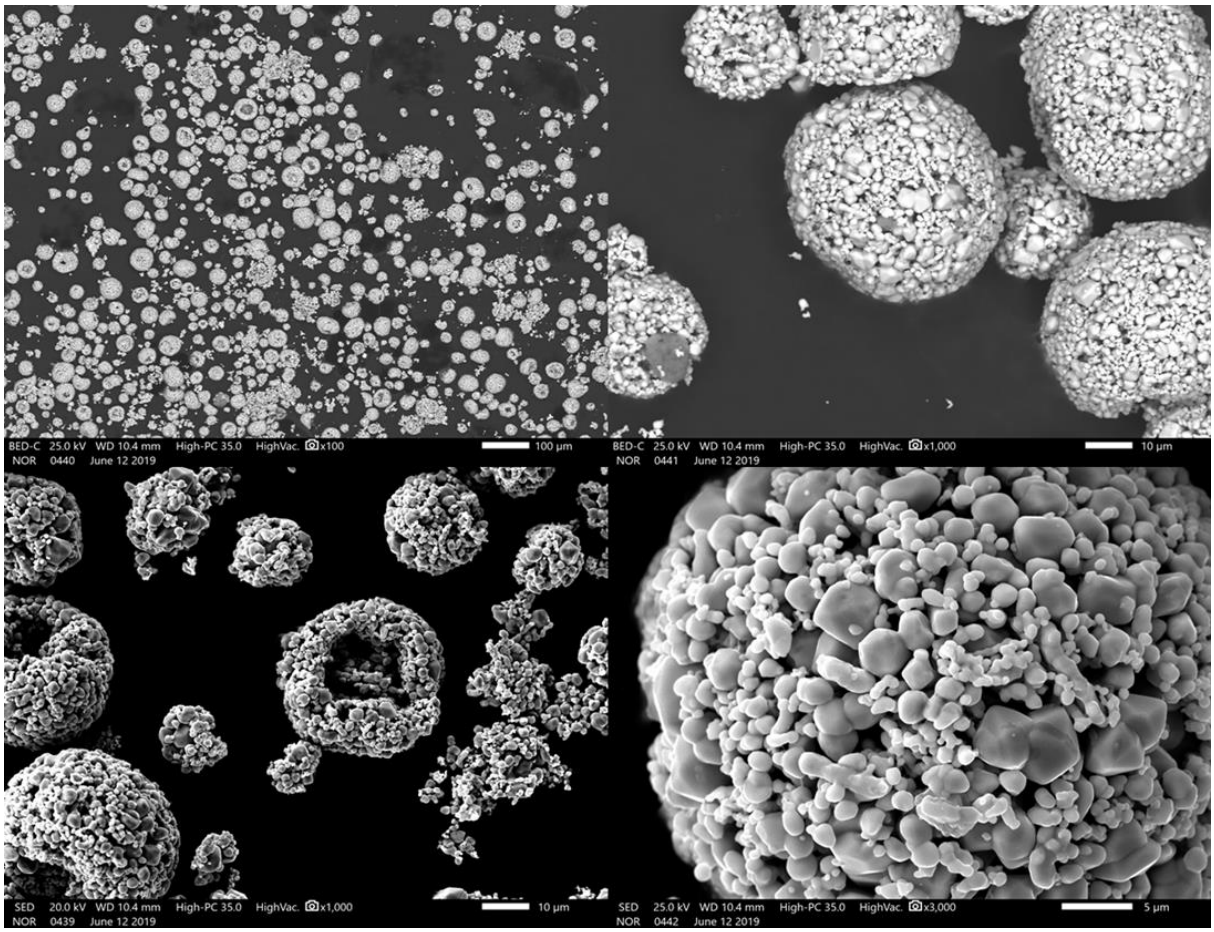

Figure 9: Upper Left: TZM 100 microns. Upper Right: TZM 10 Microns. Lower Left: TZM 10 Microns. Lower Right: TZM 5 Microns

The Camsizer indicated positive results for powder shape/size/morphology. However, when the powder was viewed through the SEM, there were several problems found with the particulates.

The particulates on the 100-micron scale are not very spherical. Zooming in to 10 microns, it is quite clear that the particulates are not spherical at all. However, the larger bodies are made up of clusters of nanoparticles sintered together making somewhat spherical bodies. It can also be seen in the upper right image that the Molybdenum and other elements making up TZM are not alloyed properly together. Zooming in further to the five-micron scale further indicates that the spherical bodies are made up of these nanoparticles (lower right). Following are images of other alloys depicting what gas atomized powder is supposed to look like.

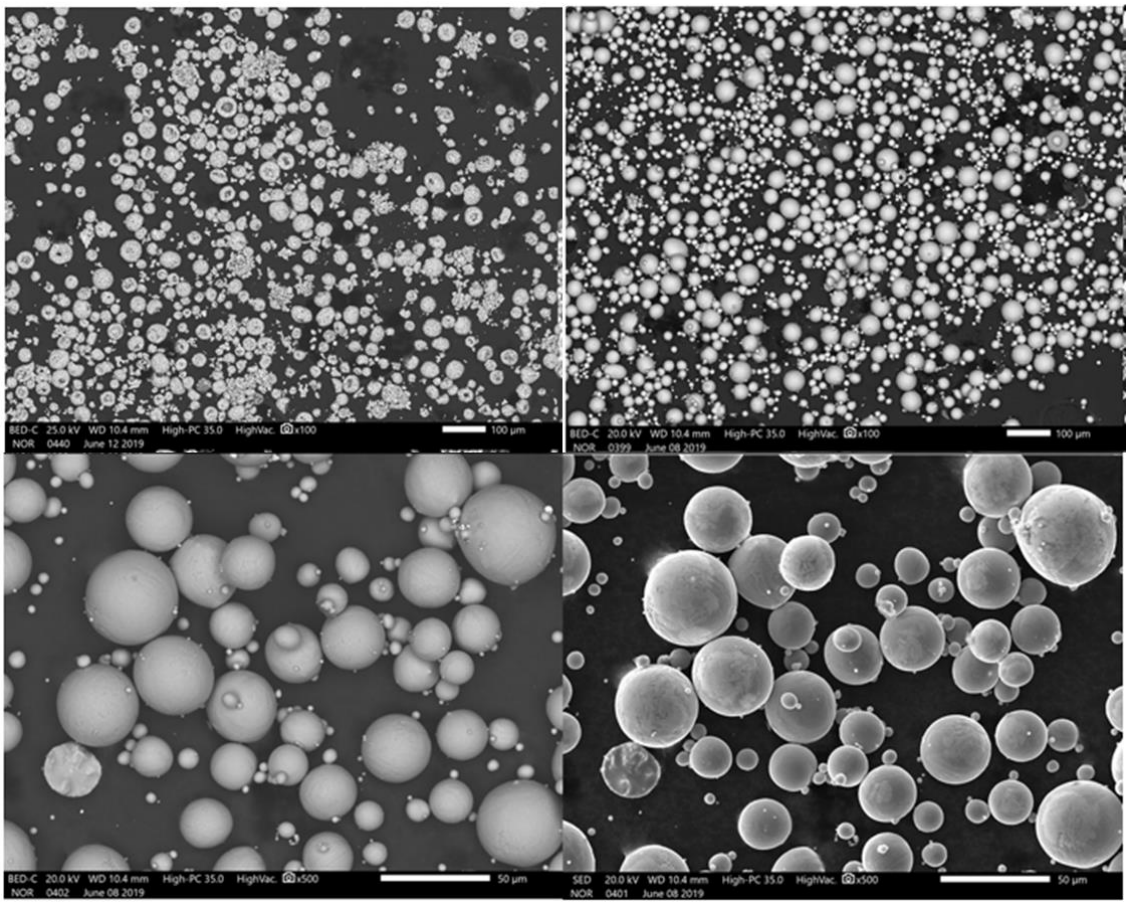

Figure 10: Upper Left: TZM 100x. Upper Right: Ti-64100x . Lower Left: Ti-64 alloy 500x BSE detector. Lower Right: Ti-64 500x SE detector

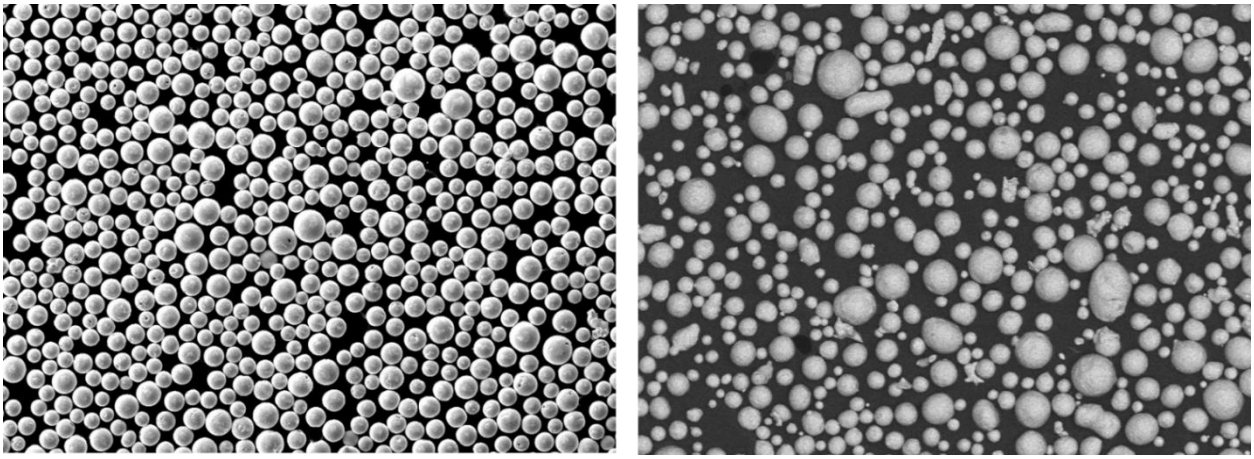

Figure 11: Left: W alloy 50 microns. Right: Cu alloy 50 microns

The images above show Titanium, Tungsten, and Copper alloys that have been previously used at the KECK center. These powders were all manufactured via gas atomization and is indicative that the TZM powder that was purchased was not gas atomized.

Tap Density Measurement: After seeing the images from the SEM, it was then desired to find the tap density of the powder. Tap density was performed via filling a small beaker of powder and collecting the initial mass and fill volume. The container was tapped against the table surface three times to settle the powder. The new fill volume was recorded and tap density was obtained. Typically for tap density, a good measurement is in the range of forty-fifty percent of the density of the solid version of the alloy.

Solid TZM has a density of 0.37 lb/in3 or 10.24 g/cm3. The recommended tap density should be in a range of 4.1 – 5.12 g/cm3. Measurements taken of the TZM powder gave a value of 2-2.5 g/cm3. This is a range of 19.5- 24.4 percent of solid TZM. Pack density is directly related to the particulate size and morphology. This measurement along with the SEM images concludes that powder most likely was not produced by gas atomization as advertised.

Conclusions to Powder Analysis: After performing all of the investigations of the analysis, it is strongly believed that the TZM powder was not produced by gas atomization. Instead, it is believed that the powder was manufactured by spray-freezing. Spray-freeze powders undergo a spheroidizing process making the granulated powder the desired spherical shape. It is believed that the purchased TZM powder underwent the spray-freezing process, but was left in an intermediate state without being spheroidized.

Images below are from a paper titled "*Densification and Crack Suppression in Selective Laser Melting of Pure Molybdenum*" The images show a pure Molybdenum powder that had been produced by freeze-spraying, and then was plasma spheroidized [45].

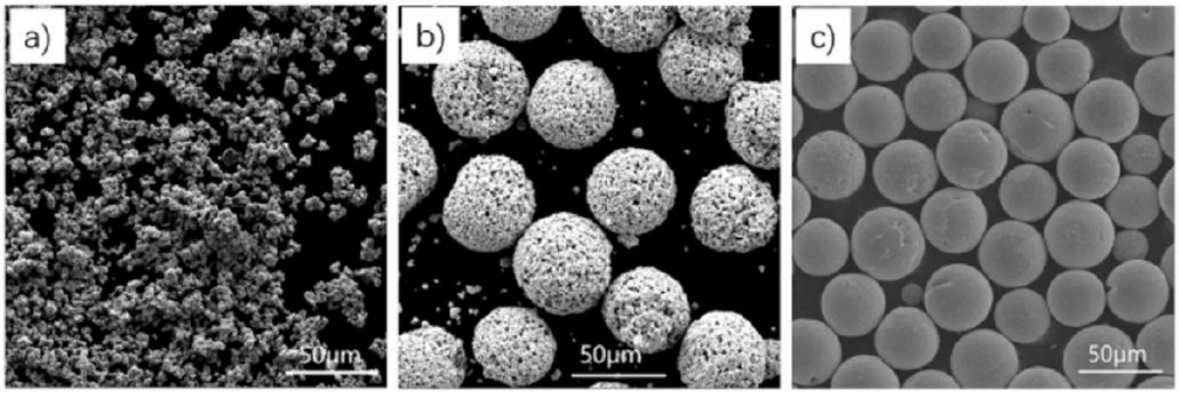

Figure 12: Right: Granulated Mo Powder. Middle: Granulated Mo Powder. Right: Spheroidized Mo Powder

In the Crack Suppression study, granulated pure Mo was spheroidized and then printed to investigate cracking. Images A and B have a resemblance to the TZM powder that was purchased. Image C depicts the Mo powder from the paper after spheroidizing. This indicates that the TZM powder on hand was not gas atomized but left in an intermediate freeze-sprayed state. Following are the EDAX APEX results obtained from the SEM.

EDAX APEX

TZM

Author: Apex User

Creation: 6/12/2019 3:54:35 PM

Sample Name: powder

Area 1

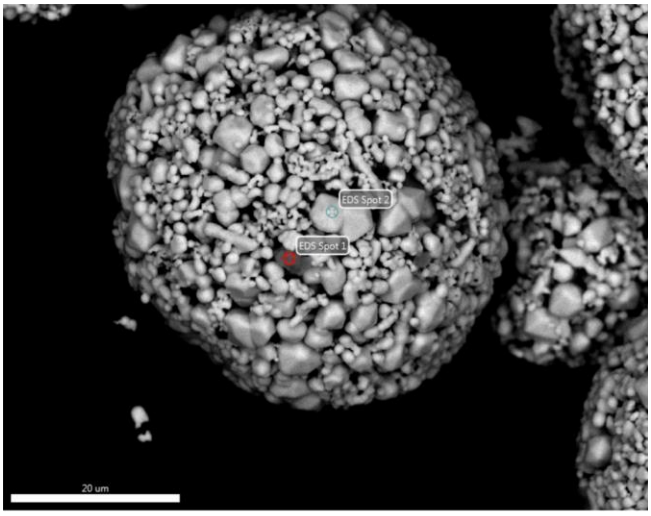

Smart Quant Results

Element	Weight %	Atomic %	Error %
TZM | powder | Area 1 | EDS Spot 1			
O K	50.84	77.61	11.09
MoL	10.47	2.67	3.7
TiK	38.69	19.73	1.76
TZM | powder | Area 1 | EDS Spot 2			
O K	2.04	11.09	52.4
MoL	97.96	88.91	1.21

Spectrum Overlay

kV: 25 Mag: 1600 Takeoff: 40.5 Live Time(s): 30 Amp Time(µs): 3.84 Resolution:(eV) 126.4

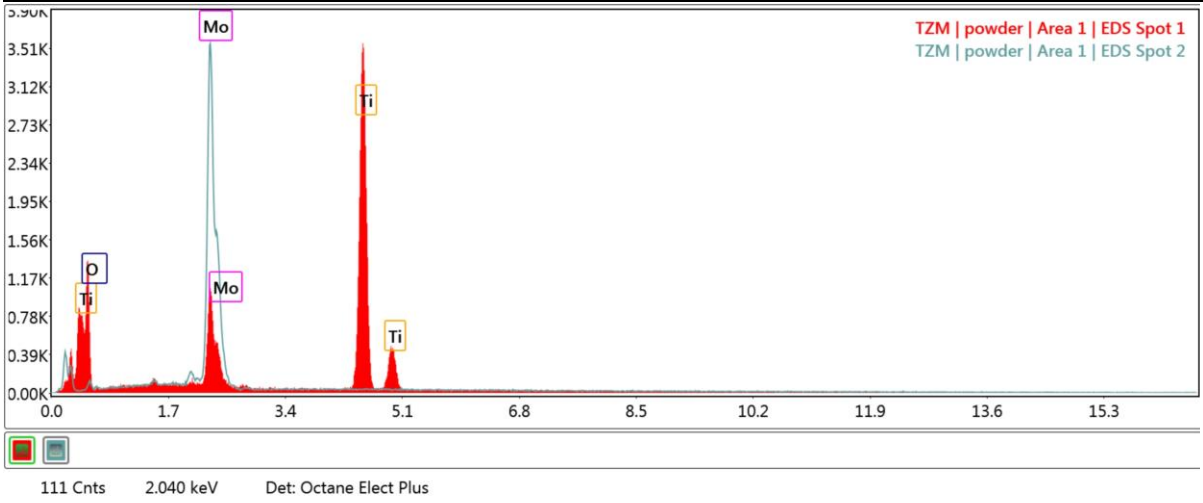

111 Cnts 2.040 keV Det: Octane Elect Plus

Figure 13: EDAX APEX Results

The powder analysis gave results that were unsettling to the researchers. Because VTS owned the powder, the responsibility of making the decision of what to do next was ultimately up to them. The researchers at UTEP believed there were other steps that could be taken, but VTS wanted to wait until American Elements corrected the powder. After repeated failed contact with American Elements, it was decided that the only option was to continue with the print series to see what results could be obtained due to time constraints.

This decision was made primarily because American Elements was identified as the only vendor that could provide the powder within the time constraints of VTS. Because TZM is not a typical alloy for L-PBF, any print results that could be obtained were considered valuable by VTS. The followings section details the results from the printing.

4.2 Parameters Set for Printing

After it was decided to print with the powder on hand, the printing parameters were reassessed and assigned for the cylinders that were going to be printed in the first series. Using the strategy of maintaining between the upper and lower boundaries of the VED value, a wide range of parameters was set for the first print series. Following is a table depicting the parameter values of the series.

Table 15: Printing Parameters

Specimen	Vector Length	Layer Thickness	Scaling	Power	Spot Size (defocus)	Hatch Spacing	Scan Speed	Volumetric Energy	Line Energy	Comments
	L	D_S	α	P_L	d_S	Δy_S	v_S	E_V	E_L	
	mm	mm		W	µm	mm	mm/s	J/mm³	J/mm²	
1	Simple Hatch	0.04	N/A	150	70	0.07	300	179	7.14	
2				150		0.07	600	89	3.57	
3				150		0.07	900	60	2.38	
4				250		0.07	600	149	5.95	
5				250		0.07	900	99	3.97	
6				300		0.07	900	119	4.76	
7				350		0.07	900	139	5.56	changed at layer 151
8				400		0.07	900	159	6.35	changed at layer 37
9				150		0.09	300	139	5.56	
10				150		0.09	600	69	2.78	
11				250		0.09	600	116	4.63	
12				250		0.09	900	77	3.09	
13				300		0.09	600	139	5.56	
14				300		0.09	900	93	3.70	
15				350		0.09	900	108	4.32	
16				400		0.09	900	123	4.94	

Table 16: Double Scan Printing Parameters

Double scan										
17,18		0.04	N/A	150	70	0.07	600	89	3.57	Added 25 layers
19,20				150		0.07	900	60	2.38	
21,22				250		0.07	900	99	3.97	
23,24				300		0.07	900	119	4.76	
25,26				300		0.09	900	93	3.70	

The tables above list the parameters that were set on the Aconity for the printing. The Aconity has the ability to change parameters mid print. Specimen that have been colored red were stopped during the print and considered failed. Green indicates a specimen that could be evaluated for density measurements after the prints. The second table displays data for specimen that received

double scans investigating re-melting of the samples during the printing. Specimen 8 was not assigned a color, because its print results were considered inconclusive.

Vector length and layer thickness were kept constant throughout all of the printing. The laser power was set at varying values from 150-400 watts. Hatch spacing varied from 0.7-0.9 millimeters, and scan speed 300-900 mm/s. This resulted in VED values that were below, above and within the range preset during the planning of the print plan. This was done so as to better evaluate the VED upper and lower bounds. The following section details the density measurements.

4.3 Density Measurements from Printed Specimen

After the specimen had been printed, it was noted that they appeared to be very porous and had poor surface roughness. The initial method chosen to measure the density of the specimen was to the Archimedes method. Due to the porosity of the specimen, it was deiced that it would be better for the cylinders to measured for volume and then weighed to get the density values. This would lead to a margin error, because it was assumed that the specimen were perfect cylinders, however the error would not be as significant as if the Archimedes method were used. Following is a table depicted the values of the density measurements.

Table 17: Density Values Found from Printed Specimen

Sample #	Height (mm)	Diameter (mm)	weight (g)	Volume mm^3	Density g/mm^3	Density g/cm^3	% to TZM
17/28	11.61	7.46	3.49	507.46	0.0069	6.8774	67.29
2	10.32	7.26	2.96	427.21	0.0069	6.9287	67.80
19/20	10.43	7.26	2.93	431.76	0.0068	6.7861	66.40
6	10.48	7.36	3.3	445.87	0.0074	7.4013	72.42
10	10.28	7.23	2.96	422.05	0.0070	7.0135	68.62
25/26	10.54	7.34	3.38	445.99	0.0076	7.5787	74.16
3	10.37	7.24	2.79	426.92	0.0065	6.5352	63.95
7	10.44	7.42	3.43	451.44	0.0076	7.5979	74.34
16	5.99	7.31	1.95	251.39	0.0078	7.7568	75.90
12	5.91	7.26	1.69	244.65	0.0069	6.9077	67.59

As stated before, the density of solid TZM is 10.22 g/cm^3. The highest value obtained from the specimen was roughly seventy-six percent of the solid value (7.76 g/cm^3). The density measurements concluded that the print results were definitely not in the range as anticipated by the KECK center. This is believed to be due largely because of the state of the powder that American Elements delivered to UTEP. The following section shows images of the printed specimen.

4.4 Density Measurements from Printed Specimen

After the specimen had been measured for density, it was desired to do some SEM imaging on the specimen that had the highest density. Specimen 16 was cross-cut, polished and prepped for SEM. However, evaluating the specimen after it had been prepped for SEM, it was conclusive that there was no use in using the microscope. Structurally, the specimen was more than subpar.

VTS collected the rest of the specimen to perform some in house testing. VTS shared some images from their analysis with UTEP, specifically specimen 7, which has the second highest density (approximately seventy-five percent of solid TZM) These images are depicted below in the following figure.

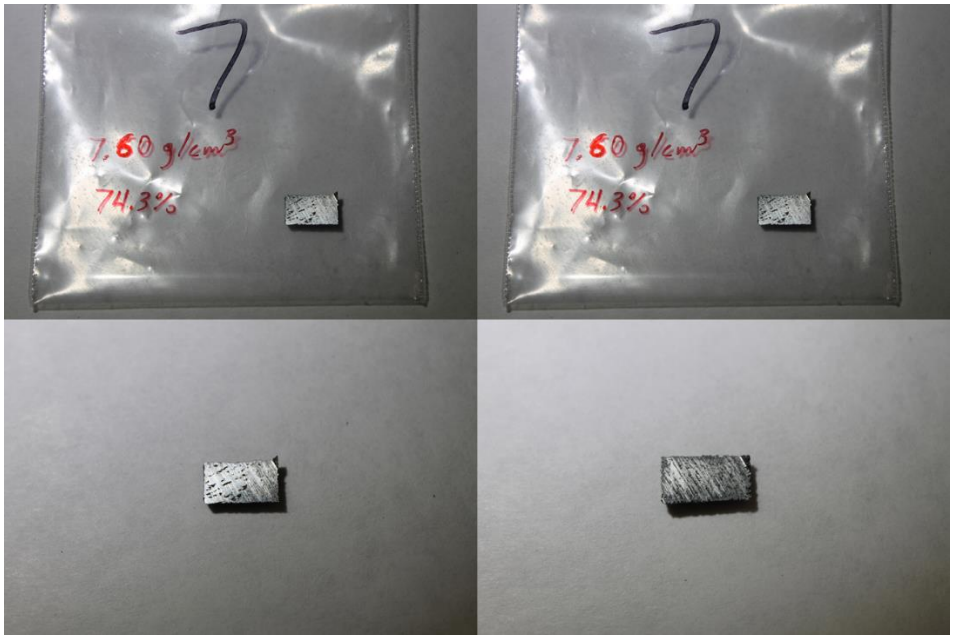

Figure 14: Upper Left: Specimen 7. Upper Right: Specimen 7. Bottom: Specimen 7

The images above along with the density data were conclusive that the print was not successful. Due to the nature of the print series and the state of the powder, it was decided to halt printing until better powder could be found.

Chapter 5: Discussions and Future Work

The focus of this thesis was to perform preliminary investigations into using Titanium Zirconium Molybdenum for additively manufacturing aerospace components. TZM was selected as a material of choice because it is a refractory metal with a high melting temperature, mechanical and physical values indicative of allowable use in harsh environments, and from previous use in the space industry. Combining additive manufacturing techniques to address the needs of a growing a space market is an interest at UTEP.

TZM is not an alloy that has had much exposure to the L-PBF community. In fact, there are several in the community that believe it is impossibly to print Molybdenum itself. The closest successful literary recording of Molybdenum printing found in this effort was the Dr. Faidel study, and his results were not promising.

This study also wished to incorporate the use of using a standardized method of assigning printing parameters. The typical guess-and-check style of L-PBF research was not an option for this effort due to limited time and resources. If successful, not only would UTEP be able to set the standard for a difficult alloy to AM, but also contribute to the standardization of L-PBF methodologies.

Unfortunately, the unsatisfactory results achieved in the printing is directly believed to be from subpar powder. Solving this is not as simple as requesting more powder from a different vendor. Due to TZM not being a usual alloy for L-PBF, finding an adequate supplier for the powder can be considered a small research venture on its own.

Specifically, the problems with the printed specimen were that they were no where near the threshold for desired density of solid TZM. During the printing process, the Aconity machine viewing window was filled with light and reflections caused by melting from the laser. This was

indicative of high oxidation levels of the powder due to its nano-sized particulates. Porosity and surface roughness could visually be seen to be way higher than what is considered to be standard. Without the proper powder, it was decided to halt printing, because results would not be indicative any further to the printability of the alloy. Simply, altering and honing would be impossible because there are too many unknowns with the current state of the alloy.

UTEP has a goal to establish refractory metal printing at the University. It is worth the trial and error of these efforts to establish a track record indicating that difficult research can be performed at UTEP. Currently, the powder is being shipped back to American Elements. American Elements is supplying UTEP with a new batch of powder, however the particulates may be outside the region desired for the Aconity (18-50 microns in diameter).

Other refractory metals that would like to be investigated by the KECK center and cSETR are Tungsten, pure Molybdenum, and Niobium. These refractory metals have more of a track record for L-PBF. Pure Molybdenum has been ordered as a part of this effort. Pure Molybdenum powder is easier to obtain, and it is believed that being able to print Molybdenum will be indicative of being able to print TZM.

In closing, the initial investigations of printing TZM are positive. The combination of the experience at UTEP, the availability of the Aconity, and the talent of the professors and research staff will result in successful results. This thesis serves as a recoding document of all work that has been done for this effort. It will serve as reference for for publications of success in AM TZM at UTEP through the partnership of the KECK Center and the cSETR. Ad Astra.

References

[1] Roop P. Following the Food. Cobblestone. 2011;32(7):4. https://search-ebscohost-com.libproxy.saumag.edu/login.aspx?direct=true&db=elr&AN=65282698&site=eds-live&scope=site. Accessed April 28, 2019.Sutton, G. P., and Biblarz, O. 2001. Rocket Propulsion Elements. 7th ed. John Wiley & Sons: New York, NY.

[2] Bob Granath (2015) The Human Desre for Explortion Leads to Discovery. Retrieved from https://www.nasa.gov/feature/the-human-desire-for-exploration-leads-to-discovery NASA's Kennedy Space Center, FloridaBrown, C. D. 1996. Spacecraft Propulsion. Washington, DC: American Institute of Aeronautics and Astronautics, Inc.

[3] Hamilton, C. J. (2011). Views of the Solar System. Retrieved from http://solarviews.com/eng/rocket.htm "UNITED STATES DEPARTMENT OF LABOR." Chemical Sampling Information | Hydrazine | Occupational Safety and Health Administration. https://www.osha.gov/dts/chemicalsampling/data/CH_245900.html.

[4] Additive Manufacturing for Space Industry Applications (2017) - From Earth to Orbit and Beyond: An Opportunity Analysis and Ten-year Forecast, SmarTech Publishing

[5] Brad Tuttle. Here's How Much it Costs for Elon Musk to Launch a SpaceX Rocket (2018). Retrieved from http://money.com/money/5135565/elon-musk-falcon-heavy-rocket-launch-cost/ Everyday Money

[6] Niaki MK, Torabi SA, Nonino F. Why manufacturers adopt additive manufacturing technologies: The role of sustainability. Journal of Cleaner Production. 2019;222:381-392. doi:10.1016/j.jclepro.2019.03.019.

[7] Asif A. Siddiqi. Competing Technologies, National(ist) Narritives, and Universal Claims (2010). An essay retrieved from NSF Essay Series, Toward a Global History of Space Exploration, pp. 425-443.

[8] Ian Christensen, Ian Lange, George Sowers, Angel Abbud-Madrid, Morgan D. Bazilian. New Policies Needed to Advance Space Mining (2019). Retrieved from Issues in Science & Technology pp. 26-30.

[9] Sheppard, Michael K.; Richardsonb, James; Taylor, Patrick A.; et al. (2017). "Radar observations and shape model of asteroid 16 Psyche". Icarus. 281: 388–403. Bibcode:2017Icar..281..388S. doi:10.1016/j.icarus.2016.08.011

[10] Bignami G. Why we need space travel. Nature. 2009;460(7253):325. doi:10.1038/460325a.

[11] Rich S. DeRoy, John G. Reed. Vulcan, Aces And Beyond: Providing Launch Services for Tomorrow's Spacecraft. Retrived from https://www.ulalaunch.com/docs/default-source/evolution/vulcan-aces-and-beyond-providing-launch-services-for-tomorrows-spacecraft-(american-astronomical-society-2016).pdf , AAS 16-052.

[12] Ajay Misra, Joe Grady, Robert Carter " Additive Manufacturing of Aerospace Propulsion Components." NASA Glenn Research Center, presented at Additve Manufacturing Conference, Pittsburgh, PA, October 01, 2015

[13] Muniz-Lerma Ja, Nommeots-Nomm A, Waters KE, Brochu M “A Comprehensive Approach to Powder Feedstock Characterization for Powder Bed Fusion Additive Manufacturing: A Case Study on AlSi7Mg.” November 27, 2018

[14] Lindemann, A.; Blumm, J. (2009). Measurement of the Thermophysical Properties of Pure Molybdenum. 3. 17th Plansee Seminar.

[15] Smallwood, Robert E. (1984). "TZM Moly Alloy". ASTM special technical publication 849: Refractory metals and their industrial applications: a symposium. ASTM International. p. 9. ISBN 978-0-8031-0203-3.

[16] Findings from Xi’an University of Architecture and Technology Reveals New Findings on Alloys and Compounds (Crack initiation mechanism in lanthanum-doped titanium-zirconium-molybdenum alloy during sintering and rolling). Chemicals & Chemistry. https://search-ebscohostcom.libproxy.saumag.edu/login.aspx?direct=true&db=edsgao&AN=edsgcl.536642864&site=eds-live&scope=site. Published 2018. Accessed June 10, 2019.V. K. Kharchenko, V. V.

[17] Bukhanovskii High-Temperature Strenght of Refractory Metals, Alloys and Composite Matierls Based on Them. Part II. Molybdenum and Niobium Alloys. Retrieved from Strength of Materials, Vol. 44, No. 6, November, 2012

[18] Studies from Xi’an University of Architecture and Technology Provide New Data on Alloys and Compounds (Electrochemical behavior and microstructural characterization of lanthanum-doped titanium-zirconium-molybdenum alloy). Chemicals & Chemistry. https://search-ebscohost com.libproxy.saumag.edu/login.aspx?direct=true&db=edsgao&AN=edsgcl.554396868&site=eds-live&scope=site. Published 2018. Accessed June 10, 2019.

[19] Tables retrieved from American Elements Product Website: https://www.americanelements.com/tzm-molybdenum-alloy-ingot

[20] Gordon L. Cann, “Spacecraft Optimized ARC Rocket” United States Patent NO: 4,548,033, Oct. 22, 1985, Laguna Beach, Calif. Appl. NO: 608,354

[21] D.M. Zube, B. Glocker, H. L. Kurtz, M. Kinnersley, and G. Matthaus “Development of a Low Power Radiatively Cooled Thermal Arcjet Thruster”

[22] Chaolin Tan, Kesong Zhou, Wenyou Ma, Bonnie Attard, Panpan Zhang, Tongchun Kuang “Selective Laser Melting of High-Performance Pure Tungsten: Parameter Desgin, Densifiaction Behavior, and Mechanical Properties” Science and Technology of Advanced Maerials Vol19, NO. 1,370-380, 2018

[23] Robert J. Cavalleri, Thomas A. Olden “Rocket Motor with Pellet and Bulk Solid Propellants” United States Patent NO: 7,685,940 B1, Mar. 30, 2010, Appl. NO: 12/053,475

[24] Gibson I, Rosen D.W., Stucker B. “Additive Manufacturing Technologies” In Rapid Prototyping to Direct Digital Manufacturing, Springer Science + Business Media; LLC: New York, NY, USA, 2010; ISBN 978-1-4419-1119-3

[25] Thijs L., Verhaeghe F., Craeghs T., Van Humbeeck J., Kruth J. P. “A Study of the Microstructural Evolution During Selective Laser Melting of Ti-6Al-4V” Acta Mater. 2010, 58, 3303-3312

[26] Mani M., Lane B., Donmez A., Feng S., Moylan S., Fresperman R., “Measurement Science Needs for Real-Time Control of Additive Manufacturing Powder Bed Fusion Process” NISTIR 8036. Available online: http://dx.doi.org/10.6028/NIST.IR.8036

[27] Faidel D., Jones D., Natour W., Behr W., “Investigation of the Selective Laser Melting Process with Molybdenum Powder” ELSEVIER Additive Manufacturing Journal 8 (2015) 88-94

[28] Bassoli E, Sola A, Celesti M, Calcagnile S, Cavallini C. Development of Laser-Based Powder Bed Fusion Process Parameters and Scanning Strategy for New Metal Alloy Grades: A Holistic Method Formulation. Materials (Basel). 2018;11(12):2356. Published 2018 Nov 22. doi:10.3390/ma11122356

[29] C. D. Boley, S. A. Khairallah, and A. M. Rubenchik, "Calculation of laser absorption by metal powders in additive manufacturing," Appl. Opt. 54, 2477-2482 (2015)

[30] Coblentz W. W. “The Reflecting Power of Various Metals” Journal of Franklin Institute Volume 170, Issue 3, (1910) Pages 169-193

[31] ASM Handbook Volume 2: Properties and Selection: Nonferrous Alloys and Special-Purpose Materials; American Society for Metals; ASM International; The Materials Information Company: Almere, The Netherlands, 1990; ISBN 978-0-87170-378-1.

[32] ASM Handbook Volume 1: Properties and Selection: Irons, Steels, and High-Performance Alloys; American Society for Metals; ASM International; The Materials Information Company: Almere, The Netherlands, 1990; ISBN 978-0-87170-377-4.

[33] Vlasea, M.L.; Lane, B.M.; Lopez, F.F.; Mekhontsev, S.; Donmez, M.A. Development of powder bed fusion additive manufacturing test bed for enhanced real time process control. In Proceedings of the International Solid Freeform Fabrication Symposium, Austin, TX, USA, 13–15 August 2015; pp. 527–539.

[34] Scipioni Bertoli, Umberto & J. Wolfer, Alexander & Matthews, Manyalibo & R. Delplanque, Jean-Pierre & M. Schoenung, Julie. (2016). On the limitations of Volumetric Energy Density as a design parameter for Selective Laser Melting. Materials & Design. 113. 10.1016/j.matdes.2016.10.037.

[35] Qingbo Jia, Dongdong Gu, Selective laser melting additive manufacturing of Inconel 718 superalloy parts: Densification, microstructure and properties Journal of Alloys and Compounds, Volume 585, 2014, pp. 713-721

[36] Metel, Alexander & Stebulyanin, Michael & Fedorov, Sergey & Okunkova, Anna. (2018). Power Density Distribution for Laser Additive Manufacturing (SLM): Potential, Fundamentals and Advanced Applications. Technologies. 7. 5. 10.3390/technologies7010005.

[37] Cheng, B.; Chou, K. Melt pool evolution study in selective laser melting. In Proceedings of the International Solid Freeform Fabrication Symposium, Austin, TX, USA, 13–15 August 2015; pp. 1182–1194.

[38] Li, L.; Lough, C.; Replogle, A.; Bristow, D.; Landers, R.; Kinzel, E. Thermal modeling of 304L stainless steel selective laser melting. In Proceedings of the ASME 2017 International Mechanical Engineering Congress and Exposition, Advanced Manufacturing, Tampa, FL, USA, 3–9 November 2017; pp. 1068–1081, ISBN 978-0-7918-5835-6.

[39] Askeland, Donald R.; Fulay, Pradeep P.; Wright, Wendelin J. (2010-06-21). The Science and Engineering of Materials (6th ed.). Cengage Learning. ISBN 9780495296027

[40] Alger, Mark. S. M. (1997). Polymer Science Dictionary (2nd ed.). Springer Publishing. ISBN 0412608707

[41] Toghyani S., Afshari E., Baniasadi E. Metal foams as flow distributors in comparison with serpentine and parallel flow fields in proton exchange membrane electrolyzer cells Electrochimica Acta, Volume 290, 2018

[42] Bauereiß, A.; Scharowsky, T.; Körner, C. Defect generation and propagation mechanism during additive manufacturing by selective beam melting. J. Mater. Process. Technol. 2014, 214, 2522–2528.

[43] Soyozo Kanbara "Method of Manufacturing High Purity Refractory Metals or Alloys." United States Patent No. US5722034A, 1994

[44] P. Tang, H & Qian, Ma & Liu, N & Zhang, Xuezhe & Y. Yang, G & Wang, Jianyih. (2015). Effect of Powder Reuse Times on Additive Manufacturing of Ti-6Al-4V by Selective Electron Beam Melting. JOM. 67. 10.1007/s11837-015-1300-4.

[45] C. D. Boley, S. C. Mitchell, A. M. Rubenchik, and S. S. Q. Wu, "Metal powder absorptivity: modeling and experiment," Appl. Opt. **55**, 6496-6500 (2016)

Curriculum Vita

Justin Vanhoose was born in Texarkana, Tx to Eddie and Kimberly Vanhoose. He graduated from Hooks High School in 2012. Immediately from Hooks High School, he attended Southern Arkansas University where he studied a hybrid degree of Engineering/Physics. At SAU, Vanhoose contributed to a number of research efforts resulting in numerous publications. He was awarded the University Scholarship, The Marilyn Hodge Engineering Scholarship, The Engineering Department Collegiate Scholarship, and upon graduation from SAU in spring of 2017, he was recognized as the Most Outstanding Engineering Student in his class. Also, while attending SAU, Vanhoose won second place at the ASEE Zone III conference in fall of 2015 for his work in implementing bio-fuel in a mini-JetCat Turbines. After graduating from Southern Arkansas University, Vanhoose attended graduate school at the University of Texas at El Paso. Here he studied Mechanical Engineering and performed research with the Center for Space Exploration and Technology Research. At UTEP, Vanhoose was a recipient of the Anita Mochen Loya Fellowship, awarded an internship for NASA Glenn Research Center LTR-O branch working on the European Service Module, and was promoted to a Staff Research Engineering position in January 2019. Upon graduation, Vanhoose was selected to work as a Fluid System Design Engineer for the United Launch Alliance working on existing technologies for Atlas and Delta, and developing technologies for the new launch vehicle, Vulcan-Centaur.